Aachen Institute for Advanced Study in Computational Engineering Science

Preprint: AICES-2007-1

27/September/2007

A Corrected XFEM Approximation without Problems in Blending Elements

T. P. Fries

RWTH AACHEN UNIVERSITY

AI CES

Financial support from the Deutsche Forschungsgemeinschaft (German Research Association) through grant GSC 111 is gratefully acknowledged.

List of AICES technical reports: http://www.aices.rwth-aachen.de/preprints

A corrected XFEM approximation without problems in blending elements

Thomas-Peter Fries

September 27, 2007

Abstract

The extended finite element method (XFEM) enables local enrichments of approximation spaces. Standard finite elements are used in the major part of the domain and enriched elements are employed where special solution properties such as discontinuities and singularities shall be captured. In elements that blend the enriched areas with the rest of the domain problems arise in general. These blending elements often require a special treatment in order to avoid a decrease in the overall convergence rate. A modification of the XFEM-approximation is proposed in this work. The enrichment functions are modified such that they are zero in the standard elements, unchanged in the elements with all their nodes being enriched, and varying continuously in the blending elements. All nodes in the blending elements are enriched. The modified enrichment function can be reproduced exactly everywhere in the domain and no problems arise in the blending elements. The corrected XFEM is applied to problems in linear elasticity and optimal convergence rates are achieved.

Contents

1 Introduction

A large number of models in continuum mechanics involve solutions that are non-smooth in local parts of the domain. There, state variables may exhibit discontinuities, singularities, or large gradients in general. For example, in solid mechanics, stresses and strains jump along material interfaces, displacements change discontinuously along cracks, and strains may be singular at a crack-tip. In fluid mechanics, high gradients are present near shocks and boundary layers.

The finite element method (FEM) is highly suited for the approximation of smooth solutions [1, 2]. It relies on the approximation properties of (mapped) polynomials [3, 4]. Special care has to be taken for approximating non-smooth solutions with the FEM. The construction of an appropriate mesh is crucial for the success of the approximation: Element edges have to align with a discontinuity and a mesh refinement is required where the solution is expected to have singularities or large gradients. Especially for the case of moving discontinuities, e.g. for the propagation of a crack or for the movement of an interface between two fluids, the maintenance of an adequate mesh is difficult or even impossible.

In contrast, the extended finite element method (XFEM) [5, 6] offers the inclusion of *a priori* known solution properties into the approximation space. The simulation is often carried out on fixed, simple (e.g. structured) meshes so that the mesh construction and maintenance is reduced to a minimum. The local enrichment of the approximation space in the XFEM is realized by means of the partition of unity concept [4, 7]. The enrichment functions employed may enable the approximation to reproduce kinks, jumps, singularities etc. exactly in local parts of the domain. References where the XFEM has been successfully employed for discontinuities are found e.g. in [5, 8, 9, 10], and for discontinuous derivatives in [11, 12, 13, 14].

Let us consider the situation where a certain enrichment function is able to capture some non-smooth solution characteristics in a local part of the domain. The nodes near this local subdomain are enriched. Then, elements result in the overall domain with all, some, or none of their element nodes being enriched. Elements with all nodes being enriched are able to reproduce the enrichment function exactly ("reproducing elements"). Elements with no enriched element nodes are standard finite elements; they are employed in those parts of the domain where the solution is smooth. Elements with some of their nodes being enriched are called "blending elements". They blend the enriched subdomain with the rest of the domain where only standard finite elements are employed.

Blending elements in the XFEM show, in general, two important properties: (i) In these elements, the enrichment function can no longer be reproduced exactly (because of a lack of a partition of unity). (ii) These elements produce unwanted terms into the approximation which cannot be compensated by the standard finite element part of the approximation. For example, a linear function can no longer be represented in a linear blending element if the enrichment introduces non-linear terms. The first aspect does not pose a significant problem in the XFEM, however, the second one may significantly reduce the convergence rate for general enrichment functions [15, 16]. Suboptimal convergence rates due to problems in blending elements have been found in [16, 17, 18].

A special treatment is in general required in blending elements in order to get rid of the unwanted terms. Among the existing approaches are those which use enhanced strain techniques or p-refinement in blending elements [15]. Another approach which adjusts the order of the finite element shape functions depending on the enrichment is discussed e.g. in [19]. Modifications of the standard XFEM approximation in order to circumvent problems in blending elements for the case of crack applications are discussed in [16]. It is noted that for the particular case of the sign- and Heaviside-enrichment, no problems in blending elements result. For solutions that involve a kink along an interface, this enrichment is often chosen although additional constraints are needed to ensure the continuity, e.g. [20, 21]. This may also be considered a special technique to avoid problems in blending elements because other enrichments are more appropriate, i.e. they do not need additional constraints, but introduce problems in blending elements. All these approaches share the property that they are not easily extended to arbitrary enrichment functions, element types, and mathematical models.

In this work, a modified definition of the XFEM approximation is proposed. Throughout this paper this is referred to as "modified XFEM" or "corrected XFEM", whereas the original definition is called "standard XFEM". Two important differences can be found in the approximations of the standard and corrected XFEM: (i) In addition to those nodes that are enriched in the standard XFEM, *all* nodes in the blending elements are enriched. That is, a complete partition of unity is present in the reproducing and blending elements. (ii) The enrichment functions of the standard XFEM are modified except in the reproducing elements. They are zero in the standard finite elements, and in the blending elements, they vary continuously between the standard and reproducing elements. The modification of the enrichment function is realized by means of a ramp function.

The corrected XFEM is able to reproduce the modified enrichment function exactly ev-

erywhere in the domain. The original enrichment function can be found exactly in the reproducing elements. Most importantly, there are no unwanted terms in the blending elements. Therefore, the corrected XFEM is able to achieve optimal convergence where the standard XFEM only achieves reduced convergence rates due to problems in the blending elements. The modified approximation of the proposed XFEM version can be applied for general enrichment functions, element types and mathematical models. The modified XFEM fits into the general framework of the standard XFEM and is, therefore, easy to implement in existing XFEM codes. The total number of degrees of freedom is slightly increased compared to the standard XFEM. The numerical results prove the success of the modified XFEM.

The paper is organized as follows: Section 2 describes the standard and corrected XFEM on a general level suited for arbitrary enrichment functions. The approximation of the standard XFEM is given in section 2.1, followed by a discussion of blending elements and the resulting problems in the standard XFEM. Section 2.3 defines the modified approximation proposed in this work. In the XFEM, it is often useful to shift enrichment functions such that the Kronecker-δ property of the approximation is maintained, this is shown in section 2.4 for the standard and modified XFEM. The generalization to more than one enrichment function is given in section 2.5. The specialization of the general approximations to the particular case of discontinuities is discussed in section 3. It starts with a short review of the levelset method for the description of discontinuities. Section 3.2 defines particular enrichment functions and the resulting approximations in the modified XFEM for strong and weak discontinuities and crack-tips. Numerical results are given in section 4 for problems in linear elasticity. Optimal convergence is achieved for a bi-material test case and crack applications. The results are significantly better than those obtained by the standard XFEM.

2 General Formulation of the Standard and Corrected XFEM

In this section, the standard and proposed modified XFEM are discussed in a general way. All applications of the XFEM can be based on the general form of the approximation shown in this section. An XFEM approximation consists of a standard finite element part and the enrichments. The enrichment terms are constructed by means of partition of unity

functions and enrichment functions that enable the approximation to capture special non-polynomial solution characteristics in local parts of the domain. A specialization of the general XFEM approximations to concrete applications such as discontinuities is discussed in the next section.

2.1 Standard XFEM

Consider an n-dimensional domain $\Omega \in \mathbb{R}^n$ which is discretized by n^{el} elements, numbered from 1 to n^{el}. I is the set of all nodes in the domain, and I_k^{el} are the element nodes of element $k \in \left\{1, \ldots, n^{\text{el}}\right\}$. A standard *extended* finite element approximation of a function $u(\boldsymbol{x})$ is of the form

$$u^h(\boldsymbol{x}) = \underbrace{\sum_{i \in I} N_i(\boldsymbol{x})\, u_i}_{\text{strd. FE approx.}} + \underbrace{\sum_{i \in I^\star} M_i(\boldsymbol{x})\, a_i}_{\text{enrichment}}, \tag{2.1}$$

where for simplicity only one enrichment term is considered. The approximation consists of a standard finite element (FE) part and the enrichment. The individual variables stand for

$$\begin{aligned}
u^h(\boldsymbol{x}) &: \text{approximated function,}\\
N_i(\boldsymbol{x}) &: \text{standard FE function of node } i,\\
u_i &: \text{unknown of the standard FE part at node } i,\\
I &: \text{set of all nodes in the domain,}\\
M_i(\boldsymbol{x}) &: \text{local enrichment function of node } i,\\
a_i &: \text{unknown of the enrichment at node } i,\\
I^\star &: \text{nodal subset of the enrichment, } I^\star \subset I.
\end{aligned}$$

The enrichment is built by *local enrichment functions* $M_i(\boldsymbol{x})$ and unknowns a_i which are defined at nodes in $I^\star \subset I$. The local enrichment functions have the form

$$M_i(\boldsymbol{x}) = N_i^\star(\boldsymbol{x}) \cdot \psi(\boldsymbol{x}), \quad \forall i \in I^\star, \tag{2.2}$$

and we call $N_i^\star(\boldsymbol{x})$ *partition of unity functions* and $\psi(\boldsymbol{x})$ *global enrichment function.* The

functions $N_i^\star(\boldsymbol{x})$ are standard FE shape functions which are not necessarily the same than those of the standard part of the approximation (2.1). These functions build a partition of unity,

$$\sum_{i \in I^\star} N_i^\star(\boldsymbol{x}) = 1, \tag{2.3}$$

in elements whose nodes are all in the nodal subset $I^\star$, see Fig. 1. In these elements, the global enrichment function $\psi(\boldsymbol{x})$ can be reproduced exactly [4]; we call these elements *reproducing elements*. In elements with only some of their nodes in $I^\star$, $N_i^\star(\boldsymbol{x})$ does not build a partition of unity, $\sum_{i \in I^\star} N_i^\star(\boldsymbol{x}) \neq 1$, see Fig. 1. As a consequence, the global enrichment function $\psi(\boldsymbol{x})$ cannot be represented exactly in these elements [15]. Throughout this paper, elements with only some of their nodes in $I^\star$ are called *blending elements*.

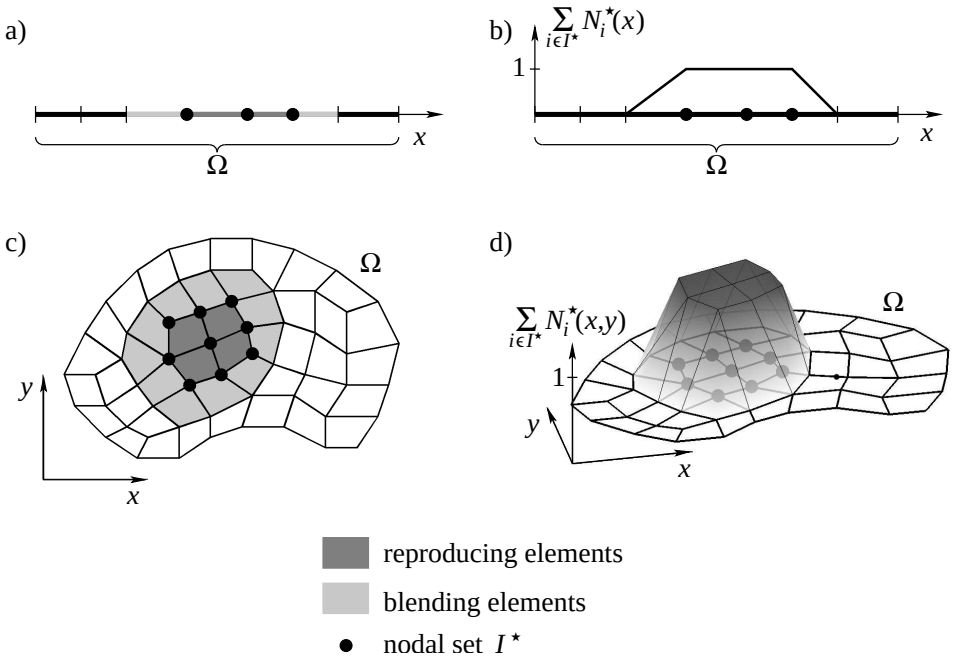

Figure 1: Discretized domains in one and two dimensions with nodal subset $I^\star$. a) and c) show the reproducing and blending elements as a consequence of the choice of $I^\star$. b) and d) show that the functions $N_i^\star(\boldsymbol{x})$ are a partition of unity in the reproducing elements, but $\sum_{i \in I^\star} N_i^\star(\boldsymbol{x}) \neq 1$ in the blending elements.

2.2 Blending Elements

Let us consider the situation in the blending elements of the standard XFEM more closely. In these elements, $\sum_{i \in I^\star} N_i^\star(\boldsymbol{x}) \neq 1$, i.e. the functions $N_i^\star(\boldsymbol{x})$ are not a partition of unity. As a consequence, the approximation is no longer able to represent the enrichment function $\psi(\boldsymbol{x})$ exactly. This fact, however, does not pose a severe problem because one is interested in capturing *local* phenomena through the enrichment. Through the choice of the nodal subset $I^\star$ one can directly prescribe the local area of the domain where the enrichment function can be represented exactly because the functions $N_i^\star(\boldsymbol{x})$ build a partition of unity there. Then, it is not necessary that also in the surrounding string of blending elements the enrichment function can be represented exactly.

Another consequence of blending elements is the introduction of unwanted terms in the approximation which, in general, cannot be compensated by the standard FE part of the approximation [15]. This can easily be seen for the following example: Consider a blending element with only one element node in $I^\star$. The approximation in this element becomes through (2.1) and (2.2)

$$u^h(\boldsymbol{x}) = \sum_{i=1}^{q} N_i(\boldsymbol{x})\, u_i + N_j^\star(\boldsymbol{x})\, \psi(\boldsymbol{x})\, a_j, \tag{2.4}$$

where q is the number of element nodes and $j \in I^\star$ is the enriched node. It becomes obvious that unless $a_j = 0$ (which deactivates the enrichment), there are, for general enrichment functions $\psi(\boldsymbol{x})$, unwanted terms resulting from $N_j^\star(\boldsymbol{x})\,\psi(\boldsymbol{x})$, which cannot be compensated by the standard FE part $\sum_i N_i(\boldsymbol{x})\, u_i$. As a consequence, in the blending elements, it is no longer possible to reproduce polynomial functions up to the order of the FE shape functions employed. For example, a linear function may no longer be reproduced for linear FE shape functions N_i if the enrichment is active ($a_j \neq 0$). Only for certain enrichment functions and/or specific choices of N_i and $N_i^\star$, these unwanted terms can be avoided.

The appearance of unwanted terms in the blending elements is much more severe than the fact that $\psi(\boldsymbol{x})$ can no longer be represented exactly. These terms can degrade the convergence of the XFEM significantly [15, 16]. A special treatment is in general required in blending elements in order to get rid of the unwanted terms. Among the existing approaches are those which use enhanced strain techniques or p-refinement in blending elements [15]. Also, an appropriate combination of the functions N_i and $N_i^\star$, e.g. quadratic FE functions

for N_i and linear FE functions for $N_i^\star$, may improve the situation for certain (e.g. polynomial) enrichment functions ψ [19]. Most of these approaches share the property that they have to be designed or at least adjusted for each enrichment function ψ individually.

It is added for completeness that it is not possible to simply set $N_i^\star(\boldsymbol{x})$ to zero in the blending elements. Then, the approximation would not introduce unwanted terms in the blending elements and would still be able to represent the enrichment function exactly in the reproducing elements. However, the resulting local enrichment functions $M_i(\boldsymbol{x})$ would be discontinuous along the element edges between the reproducing and blending elements.

2.3 Corrected XFEM

A modified formulation of the XFEM-approximation is proposed in this section. This modification avoids unwanted terms in the blending elements and still leads to continuous local enrichment functions (as long as ψ is continuous).

Let us define a modified enrichment function $\psi^{\mathrm{mod}}(\boldsymbol{x})$ as

$$\psi^{\mathrm{mod}}(\boldsymbol{x}) \;=\; \psi(\boldsymbol{x}) \cdot R(\boldsymbol{x}), \tag{2.5}$$

with $R(\boldsymbol{x})$ being a ramp function

$$R(\boldsymbol{x}) \;=\; \sum_{i \in I^\star} N_i^\star(\boldsymbol{x}). \tag{2.6}$$

A graphical representation of $R(\boldsymbol{x})$ may be seen in Fig. 1(b) and (d) for one- and two-dimensional domains. It is obvious that $\psi^{\mathrm{mod}}(\boldsymbol{x}) = \psi(\boldsymbol{x})$ in the reproducing elements (all element nodes are in $I^\star$). Furthermore, $\psi^{\mathrm{mod}}(\boldsymbol{x}) = 0$ in standard finite elements (no element nodes are in $I^\star$). In the blending elements (some element nodes are in $I^\star$), the modified enrichment function $\psi^{\mathrm{mod}}(\boldsymbol{x})$ varies continuously between $\psi(\boldsymbol{x})$ and zero. There, due to the multiplication with $R(\boldsymbol{x})$, the order of $\psi^{\mathrm{mod}}(\boldsymbol{x})$ is increased when compared to $\psi(\boldsymbol{x})$, and slightly more integration points may be appropriate for the integration.

A nodal subset $J^\star \subset I$ is introduced which consists of all element nodes of the reproducing and blending elements. In other words, $J^\star$ is the set of nodes in $I^\star$ plus their neighboring nodes (those nodes that share elements with nodes in $I^\star$). Clearly, $I^\star \subset J^\star$, which can also

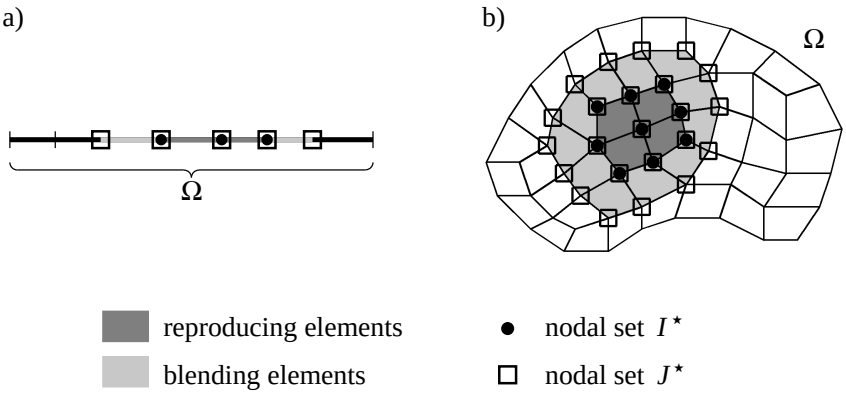

Figure 2: Discretized domains in one and two dimensions with nodal subsets $I^\star$ and $J^\star$. The definition of the reproducing and blending elements remains unchanged (based on $I^\star$).

be seen from Fig. 2. Mathematically we define $J^\star$ by help of the element set

$$\mathcal{M} = \left\{k \in \left\{1, \ldots, n^{\mathrm{el}}\right\} : I_k^{\mathrm{el}} \cap I^\star \neq \emptyset\right\} \tag{2.7}$$

as

$$J^\star = \bigcup_{k \in \mathcal{M}} I_k^{\mathrm{el}}, \tag{2.8}$$

where I_k^{el} are the element nodes of element k. The local enrichment functions are now defined as

$$M_i^{\mathrm{mod}}(\boldsymbol{x}) \;=\; N_i^\star(\boldsymbol{x}) \cdot \psi^{\mathrm{mod}}(\boldsymbol{x}), \quad \forall i \in J^\star. \tag{2.9}$$

The following modified approximation is used in the proposed corrected XFEM

$$u^h(\boldsymbol{x}) \;=\; \sum_{i \in I} N_i(\boldsymbol{x})\, u_i + \sum_{i \in J^\star} M_i^{\mathrm{mod}}(\boldsymbol{x})\, a_i. \tag{2.10}$$

The following properties for the corrected XFEM approximation are found:

- All nodes in $J^\star$ are enriched in the proposed XFEM-approximation, whereas only nodes in $I^\star \subset J^\star$ are enriched in the standard XFEM-approximation. Consequently, there are more unknowns resulting from the proposed version.
- In the proposed version of the XFEM, the enrichment function $\psi^{\mathrm{mod}}(\boldsymbol{x})$ is used

instead of $\psi(\boldsymbol{x})$.

- The modified enrichment function $\psi^{\text{mod}}(\boldsymbol{x})$ is non-zero only in the reproducing and blending elements. Most importantly, it is zero in elements with only some of their nodes in $J^\star$. That is, no unwanted terms are introduced by the proposed XFEM-approximation, and therefore, no need for any special treatment in the blending elements. In contrast, in the standard XFEM-approximation, the enrichment function $\psi(\boldsymbol{x})$ is non-zero in elements with only some of their nodes in $I^\star$, which leads to the problem of unwanted terms as discussed in section 2.2.

- In the proposed XFEM-approximation, $N_i^\star(\boldsymbol{x})$ is a partition of unity in the reproducing *and* blending elements. Consequently, the modified enrichment function $\psi^{\text{mod}}(\boldsymbol{x})$ can be reproduced exactly in all elements where this function is non-zero. In the standard XFEM, however, the enrichment function $\psi(\boldsymbol{x})$ can only be reproduced exactly in the reproducing elements but not in the blending elements.

It is noted that the definition of the reproducing and blending elements remains unchanged for the modified XFEM, i.e. based on $I^\star$. We believe that this naming is still appropriate because

- it is still only possible to reproduce $\psi(\boldsymbol{x})$ exactly in the reproducing elements. Only $\psi^{\text{mod}}(\boldsymbol{x})$ can also be reproduced exactly in the blending elements.

- the blending elements still serve the purpose to blend the approximation in the enriched part with the pure standard FE part. The difference in the corrected XFEM is that this is achieved through $\psi^{\text{mod}}(\boldsymbol{x})$ and the enrichment of *all* nodes of the blending elements, opposed to using $\psi(\boldsymbol{x})$ and enriching only *some* nodes of the blending elements as it is done in the standard XFEM.

Remark (Hierarchical blending elements) Hierarchical blending elements with the aim to compensate unwanted terms in the blending elements by increasing the polynomial order of the approximation in the blending elements are introduced in [15]. A similarity with the approach proposed in this work is the employment of additional nodes in the blending elements. However, the hierarchical blending elements are designed for polynomial enrichment functions (see [15], page 1026), whereas the modification proposed here is for general enrichment functions. The placement of the additional nodes in the blending

elements and the definition of their shape functions differ in the two approaches: In hierarchical blending elements, nodes and shape functions are introduced based on classical higher-order finite elements, whereas in this approach, only the existing nodes of the blending elements are used and their shape functions result through (2.9). It is also pointed out that the two approaches have different motivations: In hierarchical blending elements, one tries to decrease the negative effects of the unwanted terms by increasing the polynomial order in the element. This alleviates the problems of unwanted terms in blending elements but—especially for non-polynomial enrichment functions—does not fully compensate them. In contrast, the corrected XFEM avoids unwanted terms from the beginning.

2.4 Shifted Enrichment Functions

In general, standard FE shape functions have the Kronecker-δ property, i.e. $N_i(\boldsymbol{x}_j) = \delta_{ij}$. In a standard FE approximation, $u^h(\boldsymbol{x}) = \sum_i N_i(\boldsymbol{x})\, u_i$, this leads to the desirable features that

- the computed unknowns u_i are directly the sought function values of $u^h(\boldsymbol{x})$ at node i, i.e. $u^h(\boldsymbol{x}_i) = u_i$.
- the imposition of Dirichlet boundary conditions $\hat{u}(\boldsymbol{x})$ is simple: $u_i = \hat{u}(\boldsymbol{x}_i)$.

In standard XFEM approximations, see (2.1), these properties only hold for local enrichment functions that are zero at all nodes, i.e. $M_i(\boldsymbol{x}_j) = 0$, $\forall i \in I^\star$, $\forall j \in I$. This can be achieved by shifting the global enrichment function $\psi(\boldsymbol{x})$ as

$$\psi_i^{\text{shift}}(\boldsymbol{x}) \;=\; \psi(\boldsymbol{x}) - \psi(\boldsymbol{x}_i), \quad \forall i \in I^\star,$$

and using $\psi_i^{\text{shift}}(\boldsymbol{x})$ instead of $\psi(\boldsymbol{x})$ in (2.2).

For the proposed modified XFEM approximation, shifted enrichment functions with

$$M_i^{\text{mod}}(\boldsymbol{x}_j) \;=\; 0, \quad \forall i \in J^\star, \forall j \in I \tag{2.11}$$

are achieved by setting

$$\psi_i^{\text{mod,shift}}(\boldsymbol{x}) \;=\; [\psi(\boldsymbol{x}) - \psi(\boldsymbol{x}_i)] \;\cdot\; R(\boldsymbol{x}), \tag{2.12}$$

with $R(\boldsymbol{x})$ defined in (2.6). These shifted global enrichment functions are then used for the definition of M_i^{mod} as

$$M_i^{\mathrm{mod}}(\boldsymbol{x}) = N_i^{\star}(\boldsymbol{x}) \cdot \psi_i^{\mathrm{mod,shift}}(\boldsymbol{x}), \quad \forall i \in J^{\star}. \tag{2.13}$$

It is easy to show that (2.11) holds for this definition: For $i \neq j$, $N_i^{\star}(\boldsymbol{x}_j) = 0$ because these are standard FE shape functions with the Kronecker-δ property. As a result, $M_i^{\mathrm{mod}}(\boldsymbol{x}_j) = 0$. For $i = j$, $\psi(\boldsymbol{x}_j) - \psi(\boldsymbol{x}_i) = 0$, consequently $\psi_i^{\mathrm{mod,shift}}(\boldsymbol{x}_j) = 0$ and $M_i^{\mathrm{mod}}(\boldsymbol{x}_j) = 0$.

2.5 Several Enrichments

For simplicity, in the previous subsections, only one enrichment term has been considered in the XFEM-approximations, see (2.1) and (2.10). The extension to several enrichments is straightforward. The approximations for m enrichments are of the form

$$u^h(\boldsymbol{x}) = \sum_{i \in I} N_i(\boldsymbol{x}) u_i + \sum_{j=1}^{m} \sum_{i \in I_j^{\star}} M_i^j(\boldsymbol{x}) a_i^j$$

for the standard XFEM and

$$u^h(\boldsymbol{x}) = \sum_{i \in I} N_i(\boldsymbol{x}) u_i + \sum_{j=1}^{m} \sum_{i \in J_j^{\star}} M_i^{j,\mathrm{mod}}(\boldsymbol{x}) a_i^j$$

for the proposed modified XFEM. The definitions of the nodal subsets ($I_j^{\star}$ and $J_j^{\star}$) and local enrichment functions (M_i^j and $M_i^{j,\mathrm{mod}}$) are analogously to the previous subsections for each of the m enrichment terms. A shifted, standard XFEM-approximation for several enrichments becomes

$$u^h(\boldsymbol{x}) = \sum_{i \in I} N_i(\boldsymbol{x}) u_i + \sum_{j=1}^{m} \sum_{i \in I_j^{\star}} N_i^{\star}(\boldsymbol{x}) \cdot \left[\psi^j(\boldsymbol{x}) - \psi^j(\boldsymbol{x}_i)\right] \cdot a_i^j. \tag{2.14}$$

In contrast, the shifted, modified XFEM-approximation for several enrichments is

$$u^h(\boldsymbol{x}) = \sum_{i \in I} N_i(\boldsymbol{x}) u_i + \sum_{j=1}^{m} \sum_{i \in J_j^{\star}} N_i^{\star}(\boldsymbol{x}) \cdot \left[\psi^j(\boldsymbol{x}) - \psi^j(\boldsymbol{x}_i)\right] \cdot R^j(\boldsymbol{x}) \cdot a_i^j. \tag{2.15}$$

It is noted, that also for the modified XFEM-approximation, the nodal subsets $I_j^\star$ are needed for the definition of the subsets $J_j^\star$, see (2.7) and (2.8), and the ramp functions

$$R^j(\boldsymbol{x}) = \sum_{i \in I_j^\star} N_i^\star(\boldsymbol{x}).$$

3 Specialization to Discontinuities

In the previous section, the standard and modified XFEM are described on a general level without specifying the choice of the enriched nodes and the enrichment functions. In practice, the XFEM is most often used for applications with discontinuities and singularities for example near material interfaces, cracks, crack-tips, shear bands etc. In this section, the description of discontinuities by means of the levelset method is briefly mentioned. Some particularly useful enrichment functions, frequently used for strong and weak discontinuities and near crack-tips, are recalled together with a suitable choice of the enriched nodes. Throughout this paper, the partition of unity functions $N_i^\star$ are chosen identical to the shape functions of the standard FE part of the approximation, N_i.

3.1 Description of Discontinuities

The levelset method [22] is used for the description of the discontinuities in the domain. It is a numerical technique for the implicit tracking of moving interfaces and is frequently used in the context of the XFEM, see e.g. [17, 23, 24]. The basic idea is outlined as follows: A domain Ω can be decomposed into two subdomains Ω_A and Ω_B by means of a scalar function $\phi(\boldsymbol{x}) : \mathbb{R}^n \to \mathbb{R}$ which is positive in Ω_A, negative in Ω_B and zero on the interface Γ_{disc}. In this work, the signed distance function [22] is used as a particular levelset function,

$$\phi(\boldsymbol{x}) = \pm \min \|\boldsymbol{x} - \boldsymbol{x}_{\text{disc}}\|, \quad \forall \boldsymbol{x}_{\text{disc}} \in \Gamma_{\text{disc}}, \forall \boldsymbol{x} \in \Omega, \tag{3.1}$$

where the sign is different on the two sides of the discontinuity and $\|\cdot\|$ denotes the Euclidean norm.

Typically, the values of the levelset function are only stored at nodes $\phi_i = \phi(\boldsymbol{x}_i)$, and the

levelset function is interpolated by

$$\phi^h(\boldsymbol{x}) = \sum_{i \in I} N_i(\boldsymbol{x})\, \phi_i \tag{3.2}$$

using standard FE shape functions N_i as interpolation functions. The particular choice of these functions is worked out in section 3.3. It is noted that the representation of the discontinuity as the zero-level of $\phi^h(\boldsymbol{x})$ is only an approximation of the real position, which improves with mesh refinement.

Remark (Levelset method for cracks) The discontinuity described by one levelset function $\phi(\boldsymbol{x})$ is "closed", i.e. there are no end points within the domain Ω. For the case of cracks, the discontinuity ends at the crack-tip within the domain. Then, the crack path can be stored in one levelset function $\phi(\boldsymbol{x})$, and a second levelset function $\xi(\boldsymbol{x})$ can be used in order to define the position of the crack tip [23, 24], see Fig. 6.

3.2 Enrichment Functions

3.2.1 Weak Discontinuities

A function has a *kink* along weak discontinuities, i.e. it is continuous but with a discontinuous gradient. The abs-enrichment

$$\psi(\boldsymbol{x}) = \operatorname{abs}\left(\phi^h(\boldsymbol{x})\right) \tag{3.3}$$

is frequently used for capturing weak discontinuities, see e.g. [11, 12, 13, 14, 17]. The enrichment term in the standard XFEM results as

$$\sum_{i \in I^\star_{\text{abs}}} N^\star_i(\boldsymbol{x}) \cdot \left[\operatorname{abs}\left(\phi^h(\boldsymbol{x})\right) - \operatorname{abs}\left(\phi^h(\boldsymbol{x}_i)\right)\right] \cdot a_i, \tag{3.4}$$

The nodal subset $I^\star_{\text{abs}}$ contains all element nodes of elements cut by the discontinuity, see Fig. 3(a). The set of cut elements is

$$\mathcal{N} = \left\{ k \in \left\{1, \ldots, n^{\text{el}}\right\} : \min_{i \in I^{\text{el}}_k} \left(\phi^h(\boldsymbol{x}_i)\right) \cdot \max_{i \in I^{\text{el}}_k} \left(\phi^h(\boldsymbol{x}_i)\right) < 0 \right\}, \tag{3.5}$$

where I_k^{el} are the element nodes of element k. Then, $I_{\mathrm{abs}}^{\star}$ follows as

$$I_{\mathrm{abs}}^{\star} = \bigcup_{k \in \mathcal{N}} I_k^{\mathrm{el}}. \tag{3.6}$$

The enrichment term of the modified XFEM is

$$\sum_{i \in J_{\mathrm{abs}}^{\star}} N_i^{\star}(\boldsymbol{x}) \cdot \left[\mathrm{abs}\left(\phi^h(\boldsymbol{x})\right) - \mathrm{abs}\left(\phi^h(\boldsymbol{x}_i)\right) \right] \cdot R_{\mathrm{abs}}(\boldsymbol{x}) \cdot a_i, \tag{3.7}$$

where the nodal set $J_{\mathrm{abs}}^{\star}$ and the ramp function $R_{\mathrm{abs}}(\boldsymbol{x})$ are defined through Eqs. (2.6), (2.7), and (2.8) by means of the nodal set $I^{\star} = I_{\mathrm{abs}}^{\star}$.

3.2.2 Strong Discontinuities

A function shows a *jump* along strong discontinuities. Typically, the sign-enrichment is used in this case, see e.g. [5, 8, 9, 10],

$$\psi(\boldsymbol{x}) \;=\; \mathrm{sign}\left(\phi^h(\boldsymbol{x})\right). \tag{3.8}$$

It is important to note that the sign-enrichment is a special case, where also the standard XFEM does not lead to problems in blending elements. The reason is that the sign-enrichment is a constant function in the blending elements and as long as the partition of unity functions $N_i^{\star}$ are of the same or lower order than the shape functions of the standard FE part N_i, the unwanted terms in the blending elements can be compensated. For the case of the *shifted* sign-enrichment, the enrichment functions M_i in the blending elements reduce to zero which immediately shows that no unwanted terms can occur.

Therefore, for the special case of the sign-enrichment, there is no need for a modification of the standard XFEM and the enrichment for standard *and* modified XFEM is

$$\sum_{i \in I_{\mathrm{sign}}^{\star}} N_i^{\star}(\boldsymbol{x}) \cdot \left[\mathrm{sign}\left(\phi^h(\boldsymbol{x})\right) - \mathrm{sign}\left(\phi^h(\boldsymbol{x}_i)\right) \right] \cdot a_i. \tag{3.9}$$

The nodal set $I_{\mathrm{sign}}^{\star}$ is chosen in the same way than for weak discontinuities, see (3.6), i.e. $I_{\mathrm{sign}}^{\star} = I_{\mathrm{abs}}^{\star}$.

Remark (Heaviside-enrichment) It is noted that the Heaviside-enrichment is also frequently used for the enrichment in the presence of strong discontinuities. Then, the sign-function in Eqs. (3.8) and (3.9) is replaced by the Heaviside function. The same approximation space is spanned as with the sign-enrichment and the same considerations for the sign-enrichment also hold for the Heaviside-enrichment.

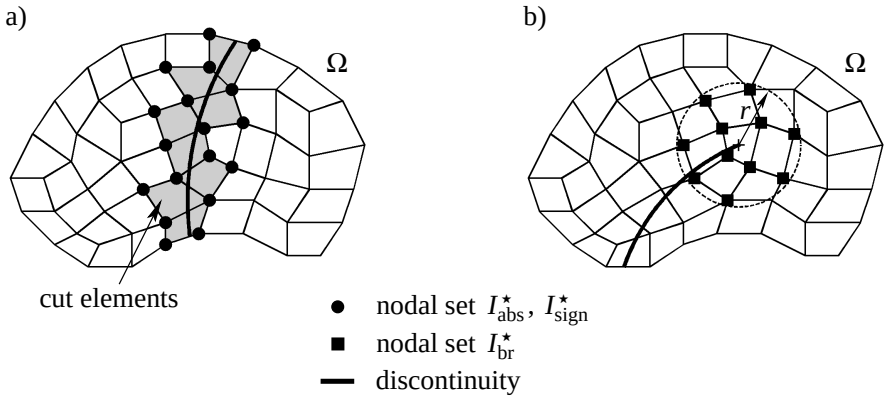

Figure 3: Choice of nodal subsets $I^\star$ for (a) the sign and abs-enrichment and (b) for the crack tip enrichment.

3.2.3 Crack Tips

At crack tips, the stresses and strains are singular. In linear elasticity in two dimensions, the following four enrichment functions are frequently used, see e.g. [5, 8, 16, 23],

$$\psi^1(r,\theta) = \sqrt{r}\sin\frac{\theta}{2}, \tag{3.10}$$

$$\psi^2(r,\theta) = \sqrt{r}\sin\frac{\theta}{2}\sin\theta, \tag{3.11}$$

$$\psi^3(r,\theta) = \sqrt{r}\cos\frac{\theta}{2}, \tag{3.12}$$

$$\psi^4(r,\theta) = \sqrt{r}\cos\frac{\theta}{2}\sin\theta. \tag{3.13}$$

The polar coordinates r and θ are according to a coordinate system defined by the geometry at the crack-tip, see Fig. 4. These four functions are frequently called branch functions and are a basis for the linear elastic crack-tip solution, see e.g. [5]. The exact solutions of the mode I and mode II crack problems, later discussed in the numerical results in section

4, are in the span of this enriched basis.

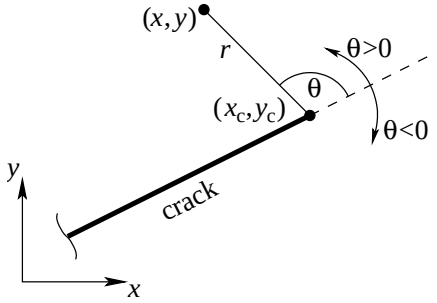

Figure 4: The polar coordinate system at the crack-tip.

With these enrichment functions, the enrichment terms in the standard XFEM approximation become

$$\sum_{j=1}^{4} \sum_{i \in I^{\star}_{\mathrm{br}}} N_i^{\star}(\boldsymbol{x}) \cdot \left[\psi^j(\boldsymbol{x}) - \psi^j(\boldsymbol{x}_i) \right] \cdot a_i^j, \tag{3.14}$$

and in the modified XFEM approximation

$$\sum_{j=1}^{4} \sum_{i \in J^{\star}_{\mathrm{br}}} N_i^{\star}(\boldsymbol{x}) \cdot \left[\psi^j(\boldsymbol{x}) - \psi^j(\boldsymbol{x}_i) \right] \cdot R_{\mathrm{br}}(\boldsymbol{x}) \cdot a_i^j. \tag{3.15}$$

The functions ψ^j are defined in (3.10) to (3.13). The nodal set $I^{\star}_{\mathrm{br}}$ ("br" stands for "branch") consists in all nodes within a certain radius r_{tip} around the crack tip at $\boldsymbol{x}_{\mathrm{c}}$, see Fig. 3(b). This is defined mathematically as

$$I^{\star}_{\mathrm{br}} \;=\; \{ i \in I : \|\boldsymbol{x}_i - \boldsymbol{x}_{\mathrm{c}}\| \leq r_{\mathrm{tip}} \}. \tag{3.16}$$

The nodal subset $J^{\star}_{\mathrm{br}}$ and ramp function $R_{\mathrm{br}}(\boldsymbol{x})$ are defined through Eqs. (2.6), (2.7), and (2.8) with $I^{\star} = I^{\star}_{\mathrm{br}}$. It is noted that in crack applications, the sign-enrichment is used along the crack path. The corresponding set of enriched nodes $I^{\star}_{\mathrm{sign}}$, see section 3.2.2, is reduced by those nodes which are already in $I^{\star}_{\mathrm{br}}$, i.e. $I^{\star}_{\mathrm{sign,red}} = I^{\star}_{\mathrm{sign}} \setminus I^{\star}_{\mathrm{br}}$.

3.3 Integration

In some elements, the local enrichment functions $M_i(\boldsymbol{x})$ and $M_i^{\mathrm{mod}}(\boldsymbol{x})$ in the standard and corrected XFEM are of a non-smooth character. There, standard Gauss-integration

performs poorly. Special integration rules have been developed for the above mentioned enrichments for discontinuities [5, 16]. They all partition reference elements into polygonal subregions for integration purposes, and place Gauss integration points in each subregion. We restrict ourselves to the situation of quadrilateral elements in two dimensions.

In elements cut by a discontinuity, a jump or kink in the local enrichment functions is present along the discontinuity. The discontinuity is described by the zero-level of the levelset function, see section 3.1. In order to ensure that the zero-level consists of (piecewise) straight lines, the quadrilateral reference element is decomposed into two triangulars. In each triangular standard linear FE shape functions are used for the interpolation of the levelset function, see (3.2). Then, it is easy to determine the polygonal subregions for the integration, which is shown in Fig. 5(a). This procedure is easily extended to three dimensions. It is noted that in all uncut elements the interpolation of the levelset function is realized by standard bi-linear FE shape functions.

In case that the element contains a crack-tip, the "almost polar integration" of [16] is employed, see also [25]. It takes the local character of the solution around the crack-tip into account. That is, the singular behavior dominated by $1/\sqrt{r}$ is integrated appropriately. This integration method maps the standard Gauss points in the quadrilateral reference element into a triangle. This is achieved by carrying out an isoparametric mapping from the reference element with two nodes being identical in the real domain. This leads to a concentration of integration points near one of the nodes of the triangle, and this node is located directly at the crack-tip. Each crack-tip element is divided into 6 triangular domains as shown in Fig. 5(b).

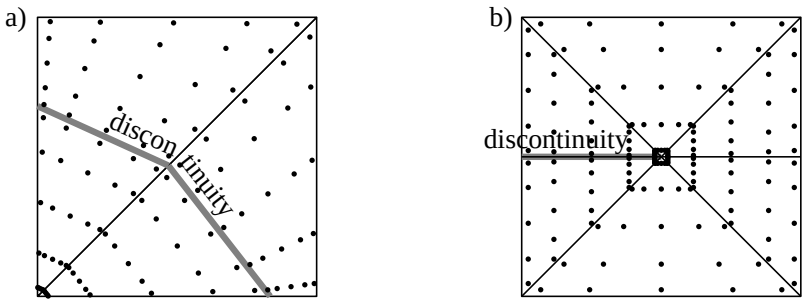

Figure 5: Dividing a fully or partially cut element into polygonal subregions for standard Gauss integration.

4 Numerical Results for Linear Elasticity

4.1 Governing Equations

A two-dimensional domain Ω with boundary Γ is considered. The boundary Γ is decomposed into the complementary sets $\Gamma_{\boldsymbol{u}}$ and $\Gamma_{\boldsymbol{t}}$. Displacements $\hat{\boldsymbol{u}}$ are prescribed along the Dirichlet boundary $\Gamma_{\boldsymbol{u}}$, and tractions $\hat{\boldsymbol{t}}$ along the Neumann boundary $\Gamma_{\boldsymbol{t}}$. Two different situations are considered. In the first case, the domain falls into two subdomains with different material properties, separated by an interface Γ_{disc}. Γ_{disc} is a closed discontinuity, i.e. it does not end within the domain, see Fig. 6(a). In the second case, the domain is cut partially by a crack Γ_c. The one-dimensional crack surface Γ_c is assumed to be traction-free. See Fig. 6(b) for a sketch of the situation.

The strong form for an elastic solid in two dimensions, undergoing small displacements and strains under static conditions, is [1, 2]

$$\nabla \cdot \boldsymbol{\sigma} = \boldsymbol{f}, \quad \text{on } \Omega \subseteq \mathbb{R}^2, \tag{4.1}$$

where $\boldsymbol{f}$ describe volume forces, and $\boldsymbol{\sigma}$ is the following stress tensor

$$\boldsymbol{\sigma} = \mathbf{C} : \boldsymbol{\varepsilon} = \lambda \left(\operatorname{tr} \boldsymbol{\varepsilon}\right) \mathbf{I} + 2\mu\boldsymbol{\varepsilon}, \tag{4.2}$$

with λ and μ being the Lamé constants. The linearized strain tensor $\boldsymbol{\varepsilon}$ is

$$\boldsymbol{\varepsilon} = \frac{1}{2}\left(\nabla \boldsymbol{u} + (\nabla \boldsymbol{u})^{\mathrm{T}}\right). \tag{4.3}$$

For the approximation of the displacements $\boldsymbol{u}$, the following test and trial function spaces $\mathcal{S}_{\boldsymbol{u}}^h$ and $\mathcal{V}_{\boldsymbol{u}}^h$ are introduced as

$$\mathcal{S}_{\boldsymbol{u}}^h = \left\{ \boldsymbol{u}^h \middle| \, \boldsymbol{u}^h \in \left(\mathcal{H}^{1h}\right)^d, \, \boldsymbol{u}^h = \hat{\boldsymbol{u}}^h \text{ on } \Gamma_{\boldsymbol{u}}, \, \boldsymbol{u}^h \text{ disc. on } \Gamma_c \right\}, \tag{4.4}$$

$$\mathcal{V}_{\boldsymbol{u}}^h = \left\{ \boldsymbol{w}^h \middle| \, \boldsymbol{w}^h \in \left(\mathcal{H}^{1h}\right)^d, \, \boldsymbol{w}^h = \boldsymbol{0} \text{ on } \Gamma_{\boldsymbol{u}}, \, \boldsymbol{w}^h \text{ disc. on } \Gamma_c \right\}, \tag{4.5}$$

where $\mathcal{H}^{1h} \subseteq \mathcal{H}^1$ is a finite dimensional Hilbert space consisting of the shape functions. The space $\mathcal{H}^1$ is the set of functions which are, together with their first derivatives, square-integrable in Ω. The discretized weak form may be formulated in the following Bubnov-

Galerkin setting [1, 2]: Find $\boldsymbol{u}^h \in \mathcal{S}_{\boldsymbol{u}}^h$ such that

$$\int_\Omega \boldsymbol{\sigma}\left(\boldsymbol{u}^h\right) : \boldsymbol{\varepsilon}\left(\boldsymbol{w}^h\right) d\Omega = \int_\Omega \boldsymbol{w}^h \cdot \boldsymbol{f}^h d\Omega + \int_{\Gamma_{\boldsymbol{t}}} \boldsymbol{w}^h \cdot \hat{\boldsymbol{t}}^h d\Gamma \quad \forall \boldsymbol{w}^h \in \mathcal{V}_{\boldsymbol{u}}^h, \tag{4.6}$$

It is shown in [6] that this weak form is equivalent to the strong form (4.1), including the traction-free condition on Γ_c.

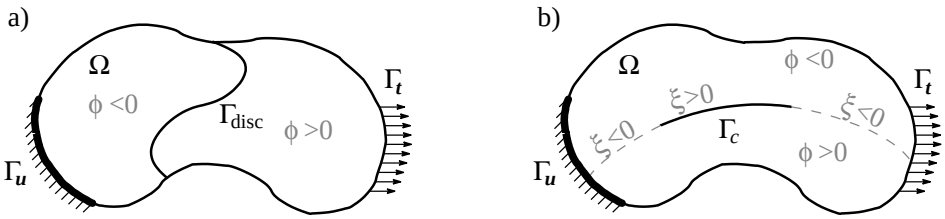

Figure 6: Structural domain with a) interface Γ_{disc} between subregions with different material properties (described by the levelset function ϕ), b) crack path Γ_c (described by the levelset functions ϕ and ξ).

4.2 One-dimensional Bar: Patch Test

In order to point out some important differences between the standard XFEM and the proposed modification, a one-dimensional bar of length l is considered, see Fig. 7(a). The problem is governed by the equation

$$k\left(x\right) \cdot u_{,xx}\left(x\right) = 0, \quad \forall x \in \left(0, l\right). \tag{4.7}$$

The stiffness $k\left(x\right)$ takes the constant value of k_1 in the left part of the bar, $x \in \left(0, x^\star\right)$, and k_2 in the right part, $x \in \left(x^\star, l\right)$, having a discontinuity at $x^\star$. The loading consists in a force F at $x = l$ and the displacement on the left is prescribed as $u\left(0\right) = 0$. The exact solution is

$$u\left(x\right) = \begin{cases} \frac{F}{k_1} \cdot x & \text{for } 0 \leq x \leq x^\star, \\ \frac{F}{k_1} \cdot x^\star + \frac{F}{k_2} \cdot \left(x - x^\star\right) & \text{for } x^\star < x \leq l, \end{cases} \tag{4.8}$$

and is illustrated schematically in Fig. 7(b). The displacement solution has a weak discontinuity, i.e. a kink, at $x^\star$. The levelset function for the description of the discontinuity is defined as

$$\phi\left(x\right) = x - x^\star.$$

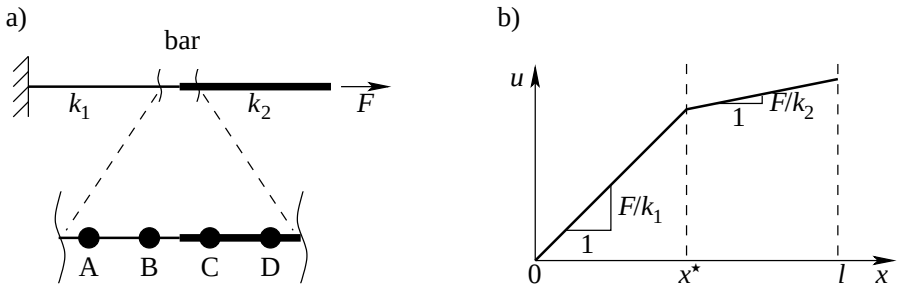

Figure 7: a) Problem statement for the one-dimensional bi-material bar with the node numbering near the discontinuity, b) shows the exact solution schematically.

Linear FE functions are employed for the shape functions N_i and $N_i^\star$. We are interested in the situation near the discontinuity, where a node numbering as shown in Fig. 7(a) is introduced. The abs-enrichment of section 3.2.1 is employed. $I^\star_{\text{abs}}$ is the set of element nodes of elements containing the discontinuity, i.e. $I^\star_{\text{abs}} = \{B, C\}$. Element $B - C$ follows as a reproducing element, and elements $A - B$ and $C - D$ as blending elements. $J^\star_{\text{abs}}$ is the set of all element nodes of the reproducing and blending elements, i.e. $J^\star_{\text{abs}} = \{A, B, C, D\}$.

For the standard XFEM, the local enrichment functions M_B and M_C are

$$M_i(x) \;=\; N_i^\star(x) \cdot \left[\text{abs}\left(\phi^h(x)\right) - \text{abs}\left(\phi^h(x_i)\right)\right] \quad \forall i \in I^\star_{\text{abs}}, \tag{4.9}$$

and are visualized in Fig. 8(c). In the reproducing elements, the piecewise linear solution with a kink at $x^\star$ can be reproduced exactly. In the blending elements, the analytical solution is linear. However, it is important to note that the local enrichment functions M_B and M_C are quadratic functions in the blending elements. That is, whenever the enrichment functions are active (a_B and a_C are non-zero), these quadratic contributions cannot be compensated by the linear finite element shape functions of the standard FE part of the approximation. And for the case that a_B and a_C are zero, the kink in the reproducing element cannot be represented exactly. This dilemma leads to a reduction of the convergence rate to first order in the L_2-norm for the standard XFEM with no special treatment in the blending elements, which has been shown in [15]. This is the same poor convergence rate that can be achieved by a standard FE approximation (without any enrichment) if the discontinuity is within an element.

For the proposed modified XFEM, the local enrichment functions are

$$M_i^{\mathrm{mod}}(x) = N_i^{\star}(x) \cdot \left[\mathrm{abs}\left(\phi^h(x)\right) - \mathrm{abs}\left(\phi^h(x_i)\right)\right] \cdot R(x) \quad \forall i \in J_{\mathrm{abs}}^{\star}. \tag{4.10}$$

It can be seen that there are more enrichment functions and consequently more unknowns a_i than for the standard XFEM, see (4.9). A graphical representation of the local enrichment functions is given in Fig. 8(d). In the reproducing elements, the situation is unchanged and the exact solution (4.8) can be reproduced exactly. In the blending elements, where the exact solution is linear, the additional local enrichment functions M_A^{mod} and M_D^{mod} are present. It can already be seen from the visualizations of the local enrichment functions in Fig. 8(d) that M_A^{mod} is able to compensate for the functional contribution of M_B^{mod} in the blending element $A-B$, and M_D^{mod} for the contribution of M_C^{mod} in the blending element $C-D$. Therefore, a linear function can be reproduced exactly in the blending elements opposed to the situation for the standard XFEM. Most importantly, this property enables the modified XFEM to reproduce the exact solution (4.8) exactly in the *overall* domain. With the modified XFEM, the exact solution is found for this test case for any number of elements (the L_2-error is of order 10^{-14}).

4.3 One-dimensional Bar: Convergence Study

A convergence study is performed for the bi-material bar of section 4.2, a problem statement is given in Fig. 9(a). A cubic line force $q(x) = x^3$ is present along the bar of length $l = 1$. The problem is governed by the equation

$$k(x) \cdot u_{,xx}(x) = -q(x), \quad \forall x \in (0,1), \tag{4.11}$$

with $k(x) = k_1 = 1$ for $0 \leq x \leq 0.5$ and $k(x) = k_2 = 10$ for $0.5 < x \leq 1$. The displacements are prescribed as $u(0) = u(1) = 0$. The exact solution is

$$u(x) = \begin{cases} -\frac{1}{320} \cdot x \cdot \frac{16x^4(k_1+k_2)-31k_1-k_2}{k_1(k_1+k_2)} & \text{for } 0 \leq x \leq 0.5, \\ -\frac{1}{320} \cdot \frac{16x^5(k_1+k_2)-31k_1x-k_2x+15(k_1-k_2)}{k_2(k_1+k_2)} & \text{for } 0.5 < x \leq 1, \end{cases} \tag{4.12}$$

and is displayed in Fig. 9(b).

For the convergence study, finite element functions of different orders have been employed in the standard (N_i) and enriched part ($N_i^{\star}$) of the XFEM approximation. Let n be the order

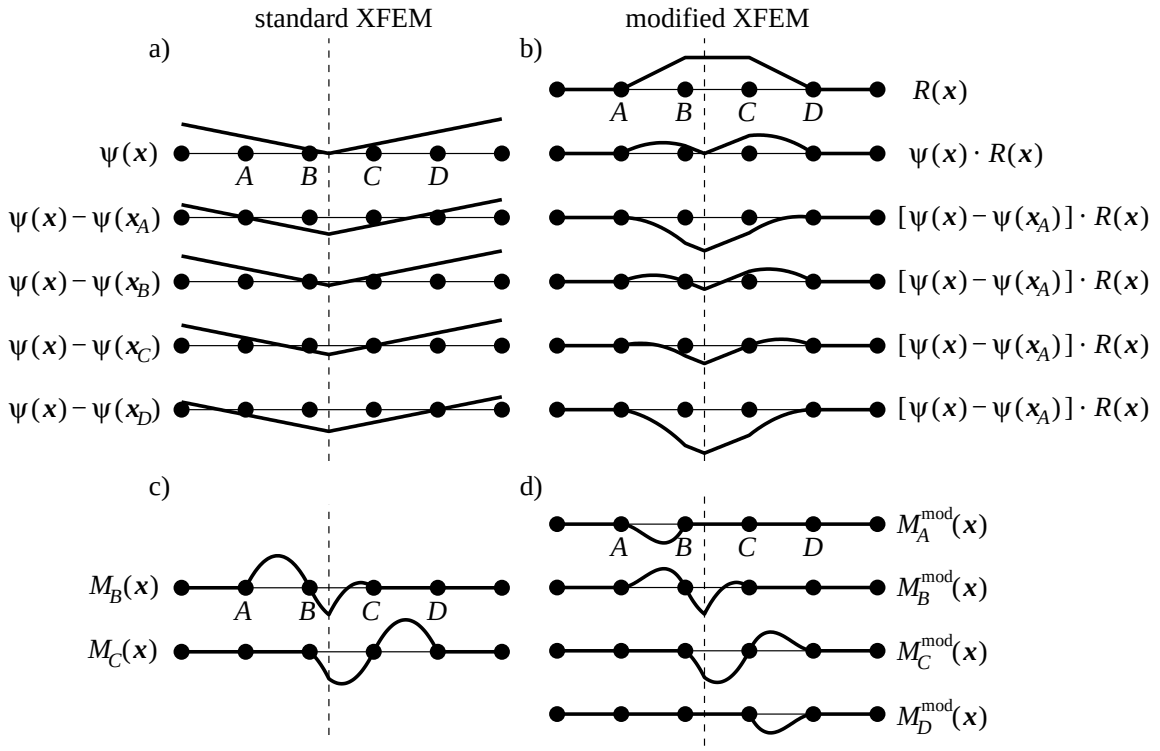

Figure 8: For the standard and modified XFEM, the (shifted) enrichment functions ψ and ψ^{mod} are shown in a) and b). The resulting local enrichment functions M_i for all $i \in I^{\star}_{\text{abs}} = \{B, C\}$ and M_i^{mod} for all $i \in J^{\star}_{\text{abs}} = \{A, B, C, D\}$ are shown in c) and d).

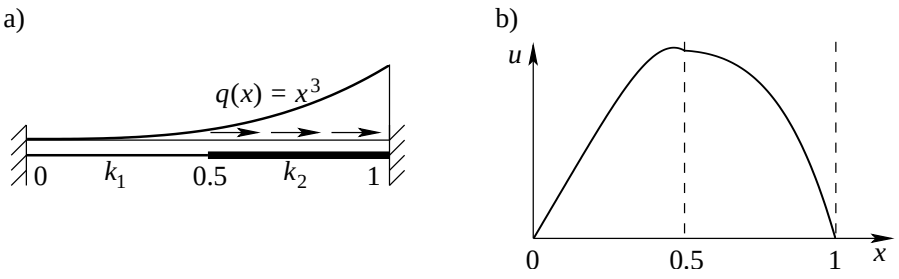

Figure 9: a) Problem statement for the one-dimensional bi-material bar with line loading, b) shows the exact solution.

of the shape functions N_i and $n^\star$ the order of the partition of unity functions $N_i^\star$. In the first study, $n = n^\star$ in the reproducing element. It is noted that $N_i^\star$ is always chosen linear in the blending elements in order to avoid linear dependencies as a result of this special enrichment (abs-enrichment and linear levelset function). The ramp function $R(x)$ results from a summation of the functions $N_i^\star$, see Eq. (2.6), i.e. it is of order $n = n^\star$. Fig. 10(a) shows that, with the corrected XFEM, optimal convergence is achieved for different orders. Because the exact solution (4.12) is a fifth-order polynomial, elements with a larger order than 4 can find the solution exactly, i.e. with machine accuracy. In contrast, the standard XFEM reduces to first order accuarcy for all types of elements, see Fig. 10(b). However, it is mentioned that optimal convergence can also be obtained for this specific enrichment in a standard XFEM approximation by choosing $n^\star = n - 1$, i.e. the order of $N_i^\star$ is one less than the order of N_i. Because then the unwanted terms in the blending elements may be compensated by the standard finite element part of the approximation.

In a second study, we set $n^\star = 1$ and only n is changed, i.e. the partition of unity functions $N_i^\star$ are kept linear. Only here, the ramp function is built by the functions N_i in contrast to $N_i^\star$, consequently $R(x)$ is of order n for this study. The results are given in Fig. 10(c). It may be seen that the rate of convergence is bounded by 3.5 in the L_2-norm. This can be explained from an analysis of the reproducing element. In the case when $n^\star = 1$ independently of n, in the reproducing element, a polynomial of order n plus a bi-linear contribution with a kink at $x = 0.5$ can be reproduced exactly. However, the exact solution (4.12) consists of *two* independent fifth order polynomials in each of the two halves which are C_0-continuous at $x = 0.5$. It is noted that the choice $n^\star = n$ enables the representation of two independent (continuous) polynomials in the reproducing element.

4.4 Two-dimensional Bi-material Problem

In this test case, a weak discontinuity is present, and the displacement field is continuous with discontinuous stresses and strains. Inside a circular plate of radius b, whose material is defined by $E_1 = 10$ and $\nu_1 = 0.3$, a circular inclusion with radius a of a different material with $E_2 = 1$ and $\nu_2 = 0.25$ is considered. The loading of the structure results from a linear displacement of the outer boundary: $u_r(b, \theta) = r$ and $u_\theta(b, \theta) = 0$. The situation is depicted in Fig. 11(a). The exact solution may be found in [17].

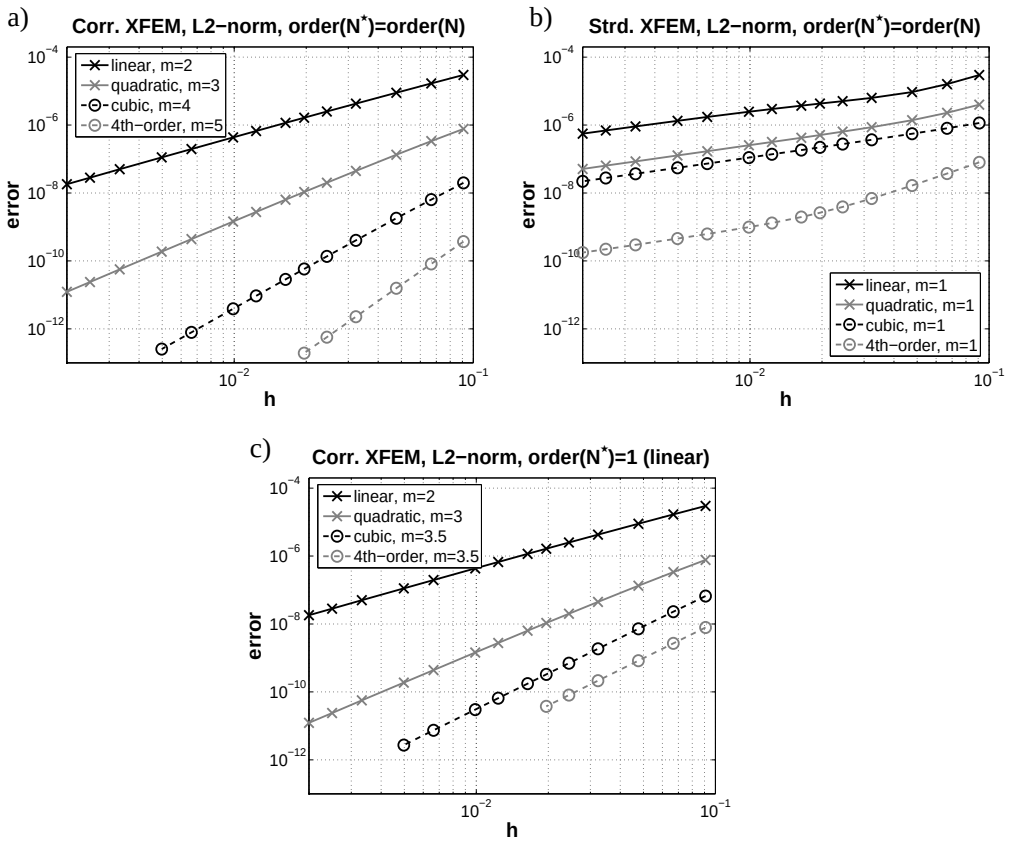

Figure 10: Convergence results for the bi-material bar with line loading, (a) and (b) choose the order of N_i and $N_i^\star$ identical in the blending elements for the corrected and standard XFEM, respectively, (c) shows results with a linear $N_i^\star$ and the corrected XFEM.

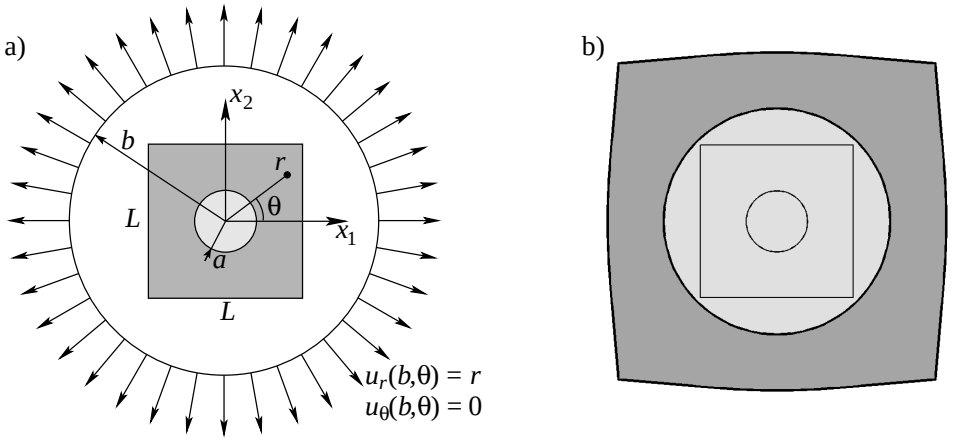

Figure 11: (a) Problem statement of the bi-material problem (the grey area is the numerical domain), (b) the exact displacement solution.

The stresses are given as

$$\sigma_{rr}(r,\theta) = 2\mu\varepsilon_{rr} + \lambda(\varepsilon_{rr} + \varepsilon_{\theta\theta}), \tag{4.13}$$

$$\sigma_{\theta\theta}(r,\theta) = 2\mu\varepsilon_{\theta\theta} + \lambda(\varepsilon_{rr} + \varepsilon_{\theta\theta}), \tag{4.14}$$

where the Lamé constants λ and μ have to be replaced by the appropriate values for the corresponding area, respectively. The strains are

$$\varepsilon_{rr}(r,\theta) = \begin{cases} (1-\frac{b^2}{a^2})\alpha + \frac{b^2}{a^2}, & 0 \le r \le a, \\ (1+\frac{b^2}{r^2})\alpha - \frac{b^2}{r^2}, & a < r \le b, \end{cases} \tag{4.15}$$

$$\varepsilon_{\theta\theta}(r,\theta) = \begin{cases} (1-\frac{b^2}{a^2})\alpha + \frac{b^2}{a^2}, & 0 \le r \le a, \\ (1-\frac{b^2}{r^2})\alpha + \frac{b^2}{r^2}, & a < r \le b, \end{cases} \tag{4.16}$$

and the displacements

$$u_r(r,\theta) = \begin{cases} \left[(1-\frac{b^2}{a^2})\alpha + \frac{b^2}{a^2}\right] r, & 0 \le r \le a, \\ (r-\frac{b^2}{r})\alpha + \frac{b^2}{r}, & a < r \le b, \end{cases} \tag{4.17}$$

$$u_\theta(r,\theta) = 0. \tag{4.18}$$

The parameter α involved in these definitions is

$$\alpha = \frac{(\lambda_1 + \mu_1 + \mu_2)\, b^2}{(\lambda_2 + \mu_2)\, a^2 + (\lambda_1 + \mu_1)\,(b^2 - a^2) + \mu_2 b^2}. \tag{4.19}$$

For the numerical model, the domain is a square of size $L \times L$ with $L = 2$, the outer radius is chosen to be $b = 2$ and the inner radius $a = 0.4 + \gamma$. The parameter γ is set to 10^{-3}, and avoids for the meshes used that the levelset function is exactly zero at a node (in this case, the discontinuity would directly cut through that node). The exact stresses are prescribed along the boundaries of the square domain, and displacements are prescribed as $u_1\,(0, \pm 1) = 0$ and $u_2\,(\pm 1, 0) = 0$. Plane strain conditions are assumed. For the XFEM simulation, the standard FE approximation for the displacements is enriched by the abs-function of the levelset function as described in section 3.2.1.

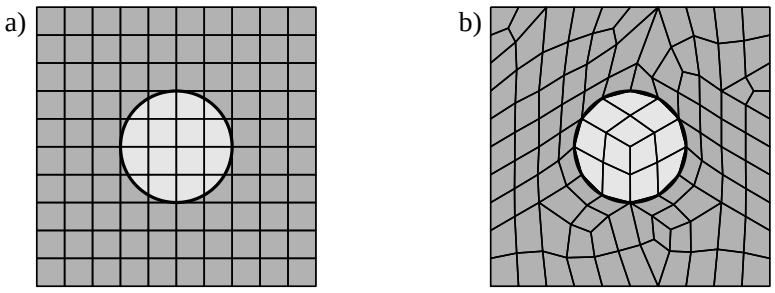

Figure 12: Meshes for the bi-material problem: (a) structured mesh used for the XFEM computations, (b) unstructured mesh aligning with the discontinuity used for the classical FEM computation.

Results are obtained for different methods: The intrinsic XFEM of [26], the standard XFEM of [5, 8, 17, ...] as described in section 2.1, and the modified XFEM are applied on structured meshes with n_d^{el} elements per dimensions. Consequently, the circular discontinuity does not align with the element edges, see Fig. 12(a). Classical FEM results are both obtained for structured meshes and special unstructured meshes as shown in Fig. 12(b), such that the discontinuity aligns with the elements edges.

For the convergence study, n_d^{el} varies between 10 and 400 elements. Fig. 13 shows the rate of convergence in the relative energy-norm and L_2-norm for the different methods employed for this test case with a weak discontinuity. The rates of convergence are obtained by means of linear regression of the data points. The *classical FEM* on structured meshes achieves first order convergence in the L_2-norm and 0.5 in the energy norm. This is due

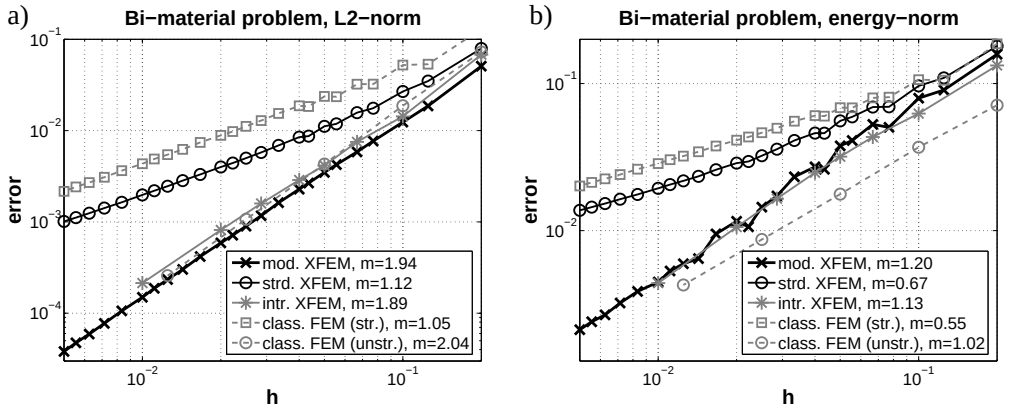

Figure 13: Convergence result for the two-dimensional bi-material problem; m is the rate of convergence.

to the lack of the standard FE shape functions to represent the kink in the displacement field appropriately. It is noted, that the integration is evaluated by the special integration technique described in section 3.3, so that the decrease in the convergence rate is not due to integration errors. The classical FEM on unstructured meshes where the discontinuity aligns with the element edges obtains optimal convergence rates of 2 in the L_2-norm and 1 in the energy-norm.

The *standard XFEM* achieves sub-optimal convergence rates. In the range of all data points shown in Fig. 13, the standard XFEM obtains convergence rates of 1.12 in the L_2-norm and 0.67 in the energy-norm. However, it may be seen that the convergence rate is not constant in the whole range of the element length h. The convergence rate becomes constant only for $n_d^{\mathrm{el}} > 50$ ($h \leq 0.02$), and approaches 1.0 in the L_2-norm and 0.5 in the energy norm. That is, although the error level is better than in the classical FEM, the convergence rate of the two methods is identical on structured meshes. A number of special techniques and enrichments have been developed in order to improve the performance of the standard XFEM, see e.g. [15, 17, 27]. The approach in [15] introduces an enhanced strain technique in order to compensate the unwanted terms in the blending elements. In [17], a smoothing technique in the blending elements is discussed. It improves the convergence rate, however, optimal values are not achieved. Another modification of the abs-enrichment is discussed in reference [27]. The resulting enrichment function represents the kink in the cut elements and is zero in the blending elements. Then, no problems in the blending elements result and optimal convergence rates may be achieved. In summary, some of the

special techniques for weak discontinuities achieve optimal convergence rates for this test case. Still, it remains that these techniques are often closely related to the particular test case and restricted to the abs-enrichment or even certain element types. Applying them to other enrichment functions, general partial differential equations (e.g. fluid models) or element types is not trivial.

The optimal rate of convergence has been achieved by the *intrinsic XFEM* in [26]. The intrinsic XFEM enriches shape functions of an approximation intrinsically so that no additional unknowns result. It follows a different methodology as the one described in section 2. The intrinsic XFEM does not show problems in blending elements.

The proposed *modified XFEM* achieves convergence rates of 1.94 in the L_2-norm and 1.2 in the energy-norm; this compares well with (or is even higher than) the optimal convergence rates. No special treatment of the blending elements is required. Compared to the intrinsic XFEM, it may be seen that not only the convergence is optimal for both methods but also the error level is very similar.

4.5 Edge-Crack Problem

In fracture mechanics, one may classify cracks into different modes [28]. In two dimensions, crack mode I and II are relevant, see Fig. 14 (b) and (c). They represent the exact displacements locally around the crack-tip. Globalizing these local solutions to the entire domain leads to the test cases computed in this section.

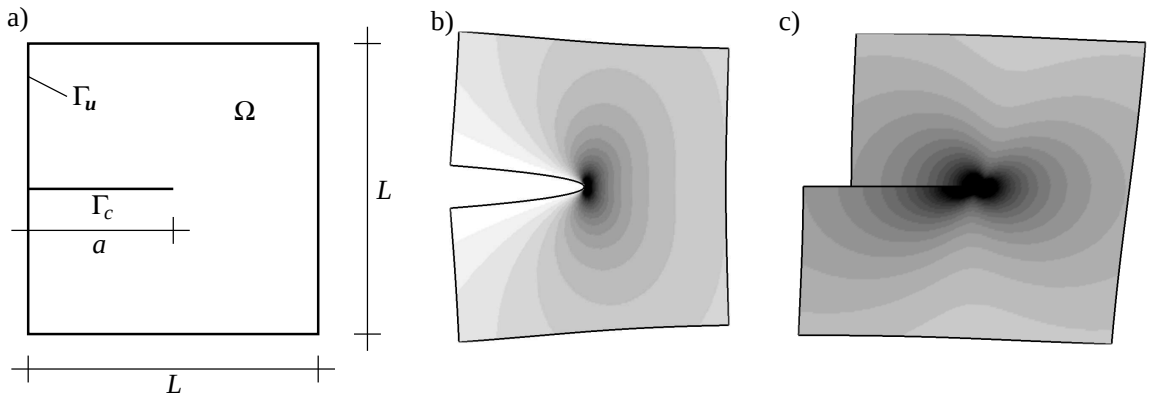

Figure 14: a) Problem statement of the edge-crack problem, b) displacements and von-Mises stresses according to the mode I and II crack.

A square domain of size $L \times L$ is considered with an edge-crack of length a, see Fig. 14(a) for a sketch. Along the boundary of the square domain, displacements are prescribed such that the well-known analytic solution of a near-tip crack field is the exact solution in the entire domain. The material is defined by $E = 10000$ and $\nu = 0.3$. The exact solution of this problem may be found e.g. in [28]. It is given in polar coordinates, see Fig. 4, for the displacements and the stress components in Table 1.

	crack mode I	crack mode II
u_1	$\frac{k_1}{2\mu}\sqrt{r/(2\pi)} \cdot \cos\frac{\theta}{2}\left[\kappa - 1 + 2\sin^2\frac{\theta}{2}\right]$	$\frac{k_2}{2\mu}\sqrt{r/(2\pi)} \cdot \sin\frac{\theta}{2}\left[\kappa + 1 + 2\cos^2\frac{\theta}{2}\right]$
u_2	$\frac{k_1}{2\mu}\sqrt{r/(2\pi)} \cdot \sin\frac{\theta}{2}\left[\kappa + 1 - 2\cos^2\frac{\theta}{2}\right]$	$-\frac{k_2}{2\mu}\sqrt{r/(2\pi)} \cdot \cos\frac{\theta}{2}\left[\kappa - 1 - 2\sin^2\frac{\theta}{2}\right]$
σ_{11}	$k_1/\sqrt{2\pi r} \cdot \cos\frac{\theta}{2}\left(1 - \sin\frac{\theta}{2}\sin\frac{3\theta}{2}\right)$	$-k_2/\sqrt{2\pi r} \cdot \sin\frac{\theta}{2}\left(2 + \cos\frac{\theta}{2}\cos\frac{3\theta}{2}\right)$
σ_{22}	$k_1/\sqrt{2\pi r} \cdot \cos\frac{\theta}{2}\left(1 + \sin\frac{\theta}{2}\sin\frac{3\theta}{2}\right)$	$k_2/\sqrt{2\pi r} \cdot \sin\frac{\theta}{2}\cos\frac{\theta}{2}\cos\frac{3\theta}{2}$
σ_{12}	$k_1/\sqrt{2\pi r} \cdot \sin\frac{\theta}{2}\cos\frac{\theta}{2}\cos\frac{3\theta}{2}$	$k_2/\sqrt{2\pi r} \cdot \cos\frac{\theta}{2}\left(1 - \sin\frac{\theta}{2}\sin\frac{3\theta}{2}\right)$

Table 1: Exact displacements and stresses for mode I and II cracks in two dimensions.

The Kolosov constant κ is defined for

$$\text{plane strain: } \kappa = 3 - 4\nu, \qquad \text{plane stress: } \kappa = \frac{3-\nu}{1+\nu}, \tag{4.20}$$

and μ is the shear modulus. The parameters k_1 and k_2 are called stress intensity factors (SIF) [28], where the indeces 1 and 2 refer to the case of a mode I or mode II crack, respectively.

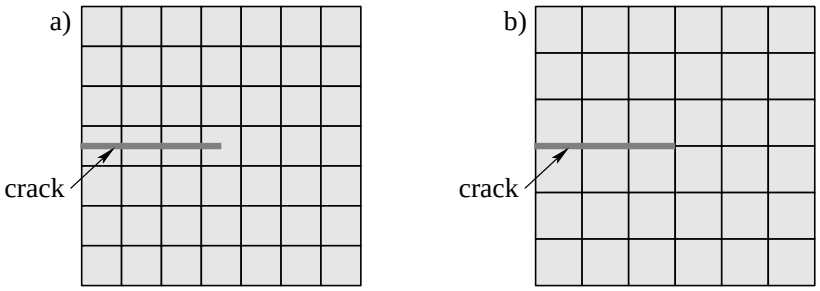

Figure 15: a) Mesh for XFEM computations, b) mesh for classical FEM simulation.

For the numerical computation, we choose $L = 2$, $a = 1$, and compute each crack mode individually. This is realized by either describing the boundary conditions according to $k_1 = 1$, $k_2 = 0$ for a pure crack mode I computation, and $k_1 = 0$, $k_2 = 1$ for the crack mode II case. Plane stress conditions are assumed. For the XFEM simulations, the nodes

around the crack-tip within an radius of r_{tip} are enriched with the branch functions as described in section 3.2.3. Along the crack, the sign-enrichment is used as discussed in section 3.2.2. Only structured meshes have been used with n_d^{el} elements per dimension. For the convergence study with different XFEM approaches, n_d^{el} is an odd number between 9 and 399, consequently, the discontinuity never aligns with the elements, see Fig. 15(a). For computations with the classical FEM, n_d^{el} is an even number between 10 and 400 so that the crack aligns with the element edges and a node is placed directly at the crack-tip, see Fig. 15(b).

4.5.1 Branch-enrichment with Constant Radius

The first results are obtained for a constant radius $r_{\text{tip}} = 0.2$ around the crack-tip. Nodes within this radius are enriched as described in section 3.2.3. Fig. 16 shows the rates of convergence in the energy and L_2-norm obtained with the standard, intrinsic, and modified XFEM and classical FEM for this test case with a strong discontinuity.

By means of the *classical FEM* only a reduced convergence order of 1 in the L_2-norm and 0.5 in the energy-norm is achieved although the crack aligns with the element edges and a node is placed at the crack-tip. The reason can be found in the singularity of the stresses and strains at the crack-tip which inhibits higher convergence rates, see also [3].

All three XFEM alternatives—standard, intrinsic, and modified XFEM—achieve optimal convergence of 2 in the L_2-norm and 1 in the energy-norm. It is surprising that for the standard XFEM, the undesired terms that are present in the blending elements of the branch-enrichment, see section 2.2, do not seem to decrease the convergence as was the case for the previous test case with the abs-enrichment. Comparing the error-levels of the results shows that for the same element size h, the proposed modified XFEM is better by a factor of 3 to 5 than the standard XFEM.

The modified XFEM enriches more unknowns than the standard XFEM. Therefore, in Fig. 17(a), the degrees of freedom (DOF) are compared between the standard and modified XFEM for the two crack modes. It can be seen that for a given accuracy, the modified XFEM requires about 3 times less degrees of freedom than the standard XFEM.

The stress intensity factors k_1 and k_2 have been evaluated numerically in a radial integration domain of radius $r = 0.6$ around the crack-tip. The interaction integral is evaluated for this purpose, see [8], and the factors should be constant, independent of the integration

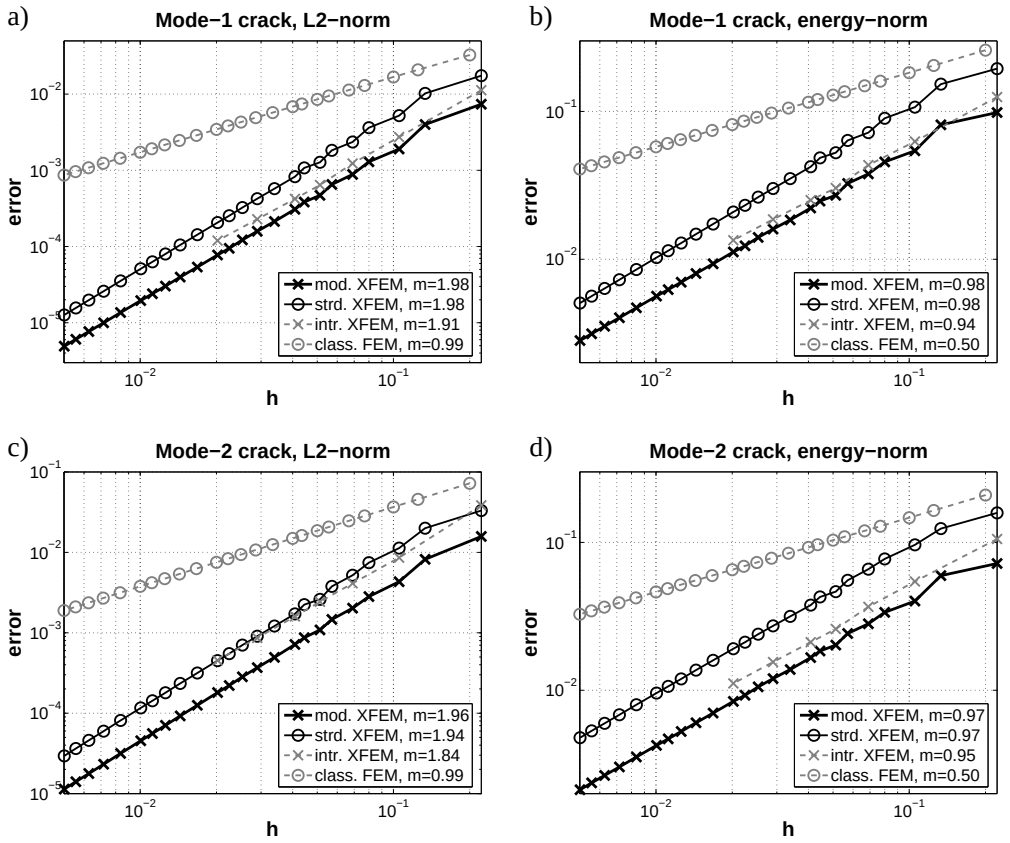

Figure 16: Convergence results in the L_2-norm and energy-norm for the mode I crack and mode II crack. The branch-enrichment is employed for nodes within a constant radius around the crack-tip.

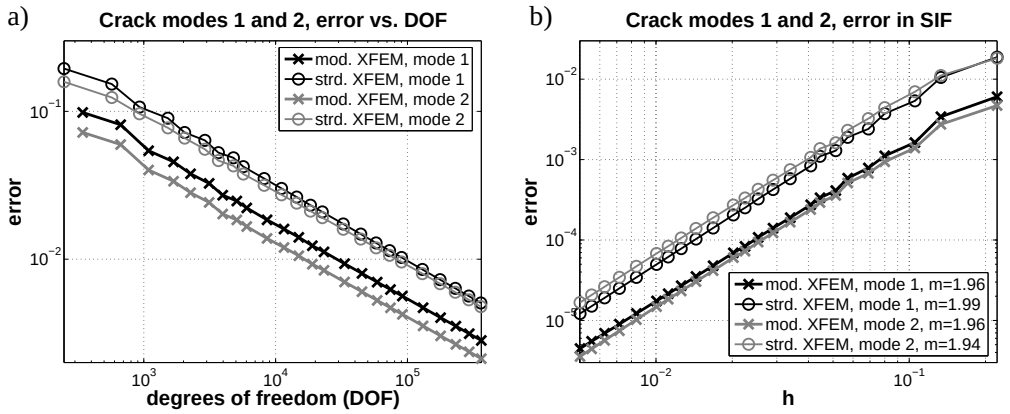

Figure 17: a) Degrees of freedom (DOF) vs. error in the energy-norm, b) mesh size h vs. error in the stress intensity factors (SIF).

domain. The results are displayed in Fig. 17(b). A convergence rate of order 2.0 towards the exact value of $k_1 = 1$ for the crack mode I case and $k_2 = 1$ for the crack mode II case may be seen. In this figure, the error in the stress intensity factors $|k_i - 1|$ is shown.

4.5.2 Branch-enrichment of the Crack-tip Element Nodes

In practice, it is often not desirable to enrich a constant radius around the crack tip, for example because a propagating crack might change its direction within r_{tip} or come too close to other cracks. It is often preferred to enrich only the element nodes of the element containing the crack-tip. In other words, r_{tip} is a function of the mesh size h and is chosen such that only the nodes of the crack-tip element are branch-enriched. The performance of the different methods is compared for this case.

The choice of the nodal subsets for the enrichments is illustrated for the standard and modified XFEM in Fig. 18. For the standard XFEM, according to section 3.2.2 and 3.2.3, all nodes in $I^\star_{\text{br}}$ are branch-enriched and all nodes in $I^\star_{\text{sign,red}}$ are sign-enriched. $I^\star_{\text{br}}$ consists of the 4 element nodes of the crack-tip element. This is referred to as "standard XFEM, version 1". For the modified XFEM, all nodes in $J^\star_{\text{br}}$ are branch-enriched according to Eq. (3.15). $J^\star_{\text{br}}$ consists through (2.7) and (2.8) of 16 nodes around the crack-tip, see Fig. 18(b). These enrichments in the standard and modified XFEM enable the resulting approximations to represent the branch-functions (3.10) to (3.13) *exactly* in the crack-tip element.

In the modified XFEM, more nodes are enriched than in the corresponding standard XFEM formulation. In this particular example, 4 nodes are branch-enriched for the standard XFEM, whereas 16 nodes are enriched for the modified XFEM. It is important to show that the results of the modified XFEM are better because no problems in blending elements are present and *not* simply because more nodes are enriched than in the standard XFEM. Therefore, it is interesting to compare the results of the modified XFEM with standard XFEM results obtained for the case that the same nodal sets are enriched. That is, a second version of the standard XFEM is analyzed where $I^\star_{\text{br}}$ consists of the 16 nodes around the crack-tip as shown in Fig. 18(c). This version is called "standard XFEM, version 2". An important difference is that the resulting approximation is able to represent the branch-functions exactly in the crack-tip element *and* its neighboring elements.

Fig. 19(a) shows the convergence results in the energy norm. It is interesting that the convergence rate is decreased to 0.5 for all XFEM-methods. That is, the branch-enrichment

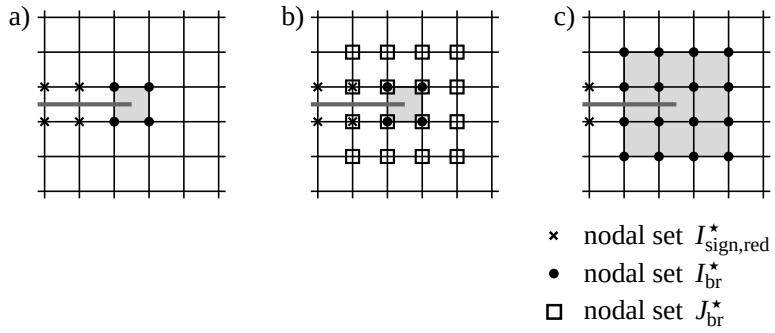

Figure 18: Nodal subsets for the enrichment for the standard XFEM, version 1 (a) and 2 (c), and the modified XFEM (b). The grey areas show where the branch functions can be represented exactly.

of nodes within a constant radius around the crack-tip as shown in section 4.5.1 is crucial for achieving optimal convergence rates in crack applications. Although the error converges at the same rate for all methods, the error-level shows significant differences. The modified XFEM performs best, followed by the intrinsic XFEM. In Fig. 19(b), the number of degrees of freedom are plotted vs. the error in the energy norm. Again, the modified XFEM achieves better results than the other XFEM versions. It is particularly interesting to note that although the same number of degrees of freedom are present for the modified XFEM and the "standard XFEM, version 2", and the branch-functions can be reproduced exactly in a larger area for the latter method, the error-level of the modified XFEM is still significantly better. We trace this back to the fact that undesired terms in the blending elements in the standard XFEM hinder better results.

Remark (Linear dependency) Let us consider the situation of a four-node quadrilateral element with all nodes being enriched by the four branch functions (3.10) to (3.13). 16 enrichment functions result in the element. It is shown in the Appendix of this work that two of these functions are linearly dependent, i.e. the mass matrix of this element has rank 14 (taking into account only the degrees of freedom related to the branch enrichment). Adding more fully enriched elements still maintains a rank deficiency of 2. Consequently, using the branch-enrichment at all nodes in the domain (global enrichment) leads to a rank-deficient system matrix in the standard XFEM. The situation changes for enriching only a local set of nodes $I^{\star}$, then, the system matrix recovers its regularity for the standard XFEM.

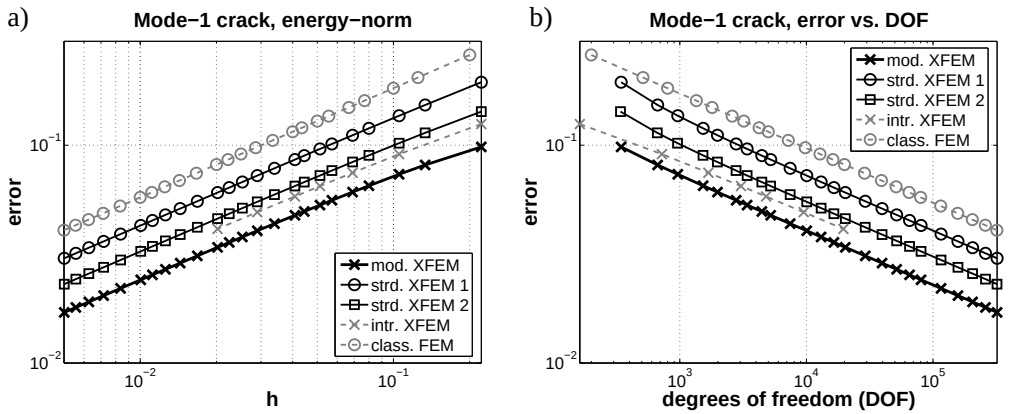

Figure 19: Convergence results in the energy-norm for branch-enrichment only in the close vicinity of the crack-tip element, a) mesh size h vs. error, b) degrees of freedom (DOF) vs. error.

In contrast, for the modified XFEM, the rank-deficiency also remains for local enrichments because all the nodes of the blending and reproducing elements are enriched, see the Appendix of this work. One can easily circumvent problems by eliminating two equations resulting for the branch-enriched degrees of freedom in the final system matrix. All results shown above have been obtained after this elimination. We conclude that this problem is not inherent in the proposed modification of the XFEM but stems from the particular case of the branch-enrichment.

Remark (Optimal convergence) We found that the following aspects have to be considered in order to obtain optimal convergence (for standard, intrinsic, and modified XFEM) in this test case:

- The integration rule in the crack-tip element is crucial for the success. The "almost polar integration", see section 3.3, is one way to integrate appropriately, see e.g. [16].
- The radius of the branch-enrichment has to be kept constant throughout the convergence study as e.g. also noted in [16, 25].
- In the standard and modified XFEM, attention has to be paid for the case where the enrichment functions $M_i(\boldsymbol{x})$ and $M_i^{\mathrm{mod}}(\boldsymbol{x})$ are non-zero along the Dirichlet boundary. Then, apart from prescribing the unknowns u_i along the Dirichlet boundary, the boundary term $\int \boldsymbol{w}^h \cdot \hat{\boldsymbol{t}}^h d\Gamma$, see Eq. (4.6), still has to be evaluated for the enrichment functions. See also [29] for imposing Dirichlet boundary conditions in the XFEM.

Remark (Other modified XFEM approximations) In [16], two modifications of the standard XFEM approximation have been proposed for the special case of crack applications. The approach of [16], section 5.1, differs from the approximation proposed in this work by the fact that only the standard nodal set $I^\star$ is enriched; suboptimal results are obtained. The other approach of [16], section 5.5, couples enriched and standard FE approximations pointwise at the nodes, its motivation is the reduction of the blending element area to zero. The formulation of the approximation and the enrichment functions are different from the proposed approximation. It is noted, that for the second approach, optimal convergence has been achieved for crack applications.

5 Summary and Conclusions

The standard formulation of XFEM approximations leads to problems in blending elements. Unwanted terms are introduced which may decrease the overall convergence. The effect of the unwanted terms in the blending elements depends on the particular enrichment chosen. For the numerical studies conducted in this work, it was found that for the abs-enrichment, the blending elements cause a severe reduction of the convergence rate to the same rate that can be achieved without any enrichment. For the branch-enrichment, the optimal convergence rate was maintained, however, the error was significantly larger than in the corresponding corrected XFEM. We conclude that blending elements have an important but hard to predict influence on the accuracy of an approximation. For the development of new enrichment functions in the context of the standard XFEM—e.g. for shocks and boundary layers in fluid mechanics—this means that an enrichment is only useful if (i) the local solution characteristics are considered appropriately *and* (ii) it can be shown (e.g. by numerical observation) that the problems in blending elements are not dominating the overall accuracy.

In contrast, for the proposed modified XFEM approximation, no problems in the blending elements result. This is achieved by a modification of the enrichment functions and an enrichment of all nodes in the blending elements. The proposed modification works for arbitrary enrichments, and is not limited to certain element types and partial differential equations. The modified XFEM approximation is easily included in existing XFEM codes. The overall number of degrees of freedom is slightly increased compared to a standard XFEM computation.

Most importantly, the results of the corrected XFEM are expected to be as good as the involved enrichment function. The better an enrichment function is suited for a particular problem, the better will be the results and no hard to predict effects in the blending elements may overshadow the accuracy.

Acknowledgements

The support of the German Research Foundation (DFG) in the frame of the Emmy-Noether-research group "Numerical methods for discontinuities in continuum mechanics" is gratefully acknowledged.

Appendix

We show that the branch-enrichment functions are linearly dependent in a bi-linear element with all element nodes being enriched. We restrict ourselves to the situation relevant in this paper: A crack is positioned at $(x_c, y_c) = (0, 0)$ with the crack angle $\theta_c = 0$. The bi-linear elements align with the x- and y-axis in the domain Ω and are defined by the left and right position x_1 and x_2 and by the bottom and top position at y_1 and y_2, respectively. See Fig. 20 for a sketch of the situation.

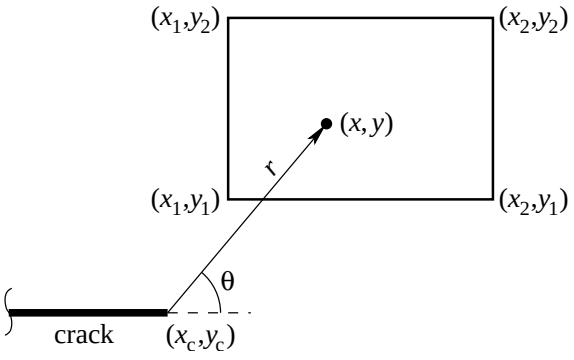

Figure 20: Element and crack situation for the proof.

There are 16 local enrichment functions $M_{ij}(\boldsymbol{x})$ in the element, defined as

$$M_{ij} = N_i^{\star}(x, y) \cdot \psi^j(r, \theta), \quad \forall i, j = 1, 2, 3, 4 \tag{5.1}$$

with ψ^j being the branch functions given by (3.10) to (3.13), and $N_i^\star$ are the bi-linear finite element shape functions

$$\begin{aligned} N_1^\star &= (1-\xi)(1-\eta), & N_3^\star &= (\xi)(\eta), \\ N_2^\star &= (\xi)(1-\eta), & N_4^\star &= (1-\xi)(\eta), \end{aligned}$$

with $\xi = (x - x_1)/(x_2 - x_1)$ and $\eta = (y - y_1)/(y_2 - y_1)$. We replace x and y by $x = r \cdot \cos\theta$ and $y = r \cdot \sin\theta$. The 16 functions (5.1) are linearly independent if

$$0 = \sum_{i=1}^{4} \sum_{j=1}^{4} N_i^\star(r,\theta) \cdot \psi^j(r,\theta) \cdot a_{ij} \tag{5.2}$$

only holds for $a_{ij} = 0 \; \forall i, j$.

However, it can be shown that the following choice of a_{ij} also fulfills (5.2):

$$a_{ij} = \begin{bmatrix} y_1x_2/y_2 & x_1x_2/y_2 + y_1 & -y_1 & -y_1x_2/y_2 + x_1 \\ y_1x_2/y_2 & x_2^2/y_2 + y_1 & -y_1 & -y_1x_2/y_2 + x_2 \\ x_2 & x_2^2/y_2 + y_2 & -y_2 & 0 \\ x_2 & x_1x_2/y_2 + y_2 & -y_2 & x_1 - x_2 \end{bmatrix}. \tag{5.3}$$

This coefficient matrix can be used in (5.2) in order to replace function M_{44} by 14 functions M_{ij}. A second coefficient matrix

$$a_{ij} = \begin{bmatrix} x_1y_1/y_2 & x_1^2/y_2 + y_1 & -y_1 & (y_2 - y_1)\,x_1/y_2 \\ x_1y_1/y_2 & x_1x_2/y_2 + y_1 & -y_1 & (y_2 - y_1)\,x_1/y_2 + x_2 - x_1 \\ x_1 & x_1x_2/y_2 + y_2 & -y_2 & x_2 - x_1 \\ x_1 & x_1^2/y_2 + y_2 & -y_2 & 0 \end{bmatrix}. \tag{5.4}$$

can be used in (5.2) in order to replace function M_{34} by the same 14 functions M_{ij} used before. This shows that 2 of the 16 equations in (5.1) are linearly dependent. The same linear combinations given above hold for the shifted enrichment in the element according to section 2.4, which gives

$$M_{ij}^{\text{shift}} = N_i^\star(\boldsymbol{x}) \cdot \left[\psi^j(\boldsymbol{x}) - \psi^j(\boldsymbol{x}_i)\right], \quad \forall i, j = 1, 2, 3, 4. \tag{5.5}$$

Furthermore, they also hold for the modified, shifted enrichment functions, i.e. for

$$M_{ij}^{\text{mod,shift}} = N_i^\star(\boldsymbol{x}) \cdot \left[\psi^j(\boldsymbol{x}) - \psi^j(\boldsymbol{x}_i)\right] \cdot R(\boldsymbol{x}), \quad \forall i,j = 1,2,3,4. \tag{5.6}$$

References

[1] T. Belytschko, W.K. Liu, and B. Moran. *Nonlinear Finite Elements for Continua and Structures*. John Wiley & Sons, Chichester, 2000.

[2] O.C. Zienkiewicz and R.L. Taylor. *The Finite Element Method*, volume 1 – 3. Butterworth-Heinemann, Oxford, 2000.

[3] G. Strang and G. Fix. *An Analysis of the Finite Element Method*. Prentice-Hall, Englewood Cliffs, NJ, 1973.

[4] I. Babuška and J.M. Melenk. The partition of unity method. *Internat. J. Numer. Methods Engrg.*, 40:727 – 758, 1997.

[5] T. Belytschko, N. Moës, S. Usui, and C. Parimi. Arbitrary discontinuities in finite elements. *Internat. J. Numer. Methods Engrg.*, 50:993 – 1013, 2001.

[6] T. Belytschko and T. Black. Elastic crack growth in finite elements with minimal remeshing. *Internat. J. Numer. Methods Engrg.*, 45:601 – 620, 1999.

[7] J.M. Melenk and I. Babuška. The partition of unity finite element method: Basic theory and applications. *Comp. Methods Appl. Mech. Engrg.*, 139:289 – 314, 1996.

[8] N. Moës, J. Dolbow, and T. Belytschko. A finite element method for crack growth without remeshing. *Internat. J. Numer. Methods Engrg.*, 46:131 – 150, 1999.

[9] J.E. Dolbow, N. Moës, and T. Belytschko. Discontinuous enrichment in finite elements with a partition of unity method. *Internat. J. Numer. Methods Engrg.*, 36:235 – 260, 2000.

[10] C. Daux, N. Moës, J.E. Dolbow, and N. Sukumar. Arbitrary branched and intersecting cracks with the extended finite element method. *Internat. J. Numer. Methods Engrg.*, 48:1741 – 1760, 2000.

[11] J. Chessa, P. Smolinski, and T. Belytschko. The extended finite element method (XFEM) for solidification problems. *Internat. J. Numer. Methods Engrg.*, 53:1959 – 1977, 2002.

[12] J. Chessa and T. Belytschko. The extended finite element method for two-phase fluids. *ASME J. Appl. Mech.*, 70:10 – 17, 2003.

[13] J.E. Dolbow and R. Merle. Solving thermal and phase change problems with the extended finite element method. *Comput. Mech.*, 28:339 – 350, 2002.

[14] H. Ji, D. Chopp, and J.E. Dolbow. A hybrid extended finite element/level set method for modeling phase transformations. *Internat. J. Numer. Methods Engrg.*, 54:1209 – 1233, 2002.

[15] J. Chessa, H. Wang, and T. Belytschko. On the construction of blending elements for local partition of unity enriched finite elements. *Internat. J. Numer. Methods Engrg.*, 57:1015 – 1038, 2003.

[16] P. Laborde, J. Pommier, Y. Renard, and M. Salaün. High-order extended finite element method for cracked domains. *Internat. J. Numer. Methods Engrg.*, 64:354 – 381, 2005.

[17] N. Sukumar, D.L. Chopp, N. Moës, and T. Belytschko. Modeling holes and inclusions by level sets in the extended finite-element method. *Comp. Methods Appl. Mech. Engrg.*, 190:6183 – 6200, 2001.

[18] F.L. Stazi, E. Budyn, J. Chessa, and T. Belytschko. An extended finite element method with higher-order elements for crack problems with curvature. *Comput. Mech.*, 31:38 – 48, 2003.

[19] J. Chessa. *The extended XFEM for free surface and two phase flow problems.* Dissertation, Northwestern University, 2003.

[20] A. Kölke. *Modellierung und Diskretisierung bewegter Diskontinuitäten in randgekoppelten Mehrfeldaufgaben.* Dissertation, Technische Universität Braunschweig, 2005.

[21] A. Kölke and A. Legay. The enriched space-time finite element method (EST) for simultaneous solution of fluid-structure interaction. *Internat. J. Numer. Methods Engrg.*, 0:submitted, 2007.

[22] S. Osher and R.P. Fedkiw. *Level Set Methods and Dynamic Implicit Surfaces*. Springer Verlag, Berlin, 2003.

[23] M. Stolarska, D.L. Chopp, N. Moës, and T. Belytschko. Modelling crack growth by level sets in the extended finite element method. *Internat. J. Numer. Methods Engrg.*, 51:943 – 960, 2001.

[24] M. Duflot. A study of the representation of cracks with level-sets. *Internat. J. Numer. Methods Engrg.*, 70:1261–1302, 2007.

[25] E. Béchet, H. Minnebo, N. Moës, and B. Burgardt. Improved implementation and robustness study of the x-fem for stress analysis around cracks. *Internat. J. Numer. Methods Engrg.*, 64:1033–1056, 2005.

[26] T.P. Fries and T. Belytschko. The intrinsic XFEM: A method for arbitrary discontinuities without additional unknowns. *Internat. J. Numer. Methods Engrg.*, 68:1358 – 1385, 2006.

[27] N. Moës, M. Cloirec, P. Cartaud, and J.F. Remacle. A computational approach to handle complex microstructure geometries. *Comp. Methods Appl. Mech. Engrg.*, 192:3163–3177, 2003.

[28] H. Ewalds and R. Wanhill. *Fracture Mechanics*. Edward Arnold, New York, 1989.

[29] N. Moës, E. Béchet, and M. Tourbier. Imposing Dirichlet boundary conditions in the extended finite element method. *Internat. J. Numer. Methods Engrg.*, 67:1641 – 1669, 2006.